Assessing the roles emission sources and atmospheric processes play in simulating $\delta^{15}N$ of atmospheric NO_x and NO_3^- using CMAQ (version 5.2.1) and SMOKE (version 4.6).

Huan Fang[†] *and Greg Michalski*[†‡]

[†]Department of Earth, Atmospheric, and Planetary Sciences Purdue University, 550 Stadium Mall Drive, West Lafayette, IN 47907, United States

[‡]Department of Chemistry, Purdue University, 560 Oval Drive, West Lafayette, IN 47907, United States

Correspondence: Huan Fang, fang63@purdue.edu

Keywords: isotope, nitrogen, atmospheric NOx, atmospheric nitrate, NOx emission sources, emission inventory, emission input dataset, atmospheric processes, disperse, mixing, transport, chemical transport model, 3D CTM, NEI, SMOKE, CMAQ

Style Definition: Comment Text: Font: (Default) Cambria, (Asian) PMingLiU, (Asian) Chinese (Taiwan)

Style Definition: Comment Subject: Font: (Default) Cambria, (Asian) PMingLiU, 12 pt, Not Bold, (Asian) Chinese (Taiwan)

Style Definition: Balloon Text: Font: (Asian) PMingLiU, (Asian) Chinese (Taiwan)

Style Definition: Footer: Font: (Default) Cambria, (Asian) PMingLiU, (Asian) Chinese (Taiwan)

Style Definition: List Paragraph: Font: (Default) +Body (Calibri), (Asian) +Body Asian (PMingLiU), Indent: Left 0 ch, Don't add space between paragraphs of the same style

Style Definition: Header: Font: (Default) PMingLiU, (Asian) PMingLiU, (Asian) Chinese (Taiwan)

Deleted: Simulating

Formatted: Font: 14 pt, Font color: Auto

Formatted: Font: 14 pt

Formatted: Font: 14 pt, Font color: Auto

Deleted: in

Formatted: Font: 14 pt

Formatted: Font: 14 pt

Deleted: , based on ^{15}N incorporated

Formatted: Font: 14 pt, Font color: Black

Formatted: Font: 14 pt

Formatted: Font: 14 pt

Deleted: and WRF version 4.0 for assessing the role atmospheric processes plays in controlling the isotopic composition of NO_x, NO_y, and atmospheric nitrate

Formatted: Font: 14 pt

Formatted: Font: Not Italic

Formatted: None

Formatted: Font: Italic

Formatted: Font: Italic

Formatted: Normal

Formatted: Not Superscript/ Subscript

Deleted: fang63@purdue.edu

Abstract

Nitrogen oxides (NO_x = nitric oxide (NO) + nitrogen dioxide (NO_2)) are important trace gases that affect atmospheric chemistry, air quality, and climate. Contemporary development of NO_x emissions inventories is limited by the understanding of the roles of vegetation (net NO_x source or net sink), gasoline and diesel in vehicle emissions, and the application of NO_x emission control technologies. The nitrogen stable isotope composition ($\delta^{15}N$) of NO_x is an effective tool to evaluate the accuracy of the NO_x emission inventories, which are based on different assumptions. In this study, we traced the changes in $\delta^{15}N$ values of NO_x along the "journey" of atmospheric NO_x, driven by atmospheric processes after different sources emit NO_x to the atmosphere. The ^{15}N was incorporated into the emission input dataset, generated from the US EPA trace gas emission model SMOKE (Sparse Matrix Operator Kernel Emissions). Then the ^{15}N incorporated emission input dataset was used to run CMAQ (the Community Multiscale Air Quality Modeling System). The simulated spatiotemporal patterns in NO_x isotopic composition for both SMOKE outputs and CMAQ outputs were compared with corresponding atmospheric measurements in West Lafayette, Indiana, USA. By enhancing NO_x deposition, we simulated the expected $\delta^{15}N$ of NO_3^- assuming no isotope fractionation during chemical conversion or deposition. These simulations were compared to $\delta^{15}N$ of NO_3^- in NADP sites. The results indicate the potential underestimation of emissions from soil, livestock waste, off-road vehicles, and natural gas power plants and the potential overestimation of emissions from on-road vehicles and coal-fired power plants, if only considering the difference in NO_x isotopic composition for different emission sources. The estimation of atmospheric $\delta^{15}N(NO_x)$ using CMAQ shows better agreement (by ~3‰) with observations than using SMOKE (Sparse Matrix Operator Kernel Emissions), due to the consideration of mixing, dispersion, transport, and deposition of NO_x emission from different sources.

Formatted: Font: 12 pt

Deleted: Despite the importance

Deleted: , there are significant uncertainties in NO_x emission …

Deleted: . After NO_x from different sources

Deleted: emitted into the atmosphere, its composition will change due to atmospheric processes. In this study, we used

Deleted: ($\delta^{15}N$(

Deleted:)) to trace

Deleted: by incorporating

Deleted: prepared from the previous companion research (Fang & Michalski, 2020)

Deleted: that the

Formatted: Font color: Auto

Formatted: Font: 11 pt

Deleted: disperse

Formatted: Font: Not Bold, Font color: Black

1. Introduction

NO_x are important trace gases that affect atmospheric chemistry, air quality, and climate ($NO_x = NO + NO_2$). The main sources of tropospheric NO_x are emissions from vehicles, power plants, agriculture, livestock waste, as well as the natural by-product of nitrification and denitrification occurring in soil, and lightning (Galloway, et al., 2004). The NO_x photochemical cycle generates OH and HO_2 radicals, organic peroxy radicals (RO_2), and ozone (O_3), which ultimately oxidize NO_x into NO_y ($NO_y = NO_x + HONO + HNO_3 + HNO_4 + N_2O_5$ + other N oxides). During the photochemical processes that convert NO_x to NO_y, ground-level concentrations of O_3 become elevated and secondary particles are generated. Secondary aerosols in turn affect cloud physics, enhancing the reflection of solar radiation (Schwartz, 1996) and are hazardous to human health (Lighty et al., 2000). Thus, the importance of NO_x in air quality, climate, and human and environmental health makes understanding the spatial and temporal variation in the sources of NO_x a vital scientific question.

Despite years of research, however, there are still several significant uncertainties in the NO_x budget. About 15% of global NO_x emissions, ranging from 6.6 to 21 Tg N yr^{-1}, is derived from global soil NO_x emissions yet evaluating and verifying emission rates using both laboratory and field measurements is still a challenge (Jaeglé et al., 2005; Yan et al., 2005; Stehfest and Bouwman, 2006; Hudman et al., 2012). Soil NO_x emissions vary by different biome types, meteorological conditions, and soil physicochemical properties. The application of N fertilizer also has a strong effect on soil NO_x emissions, which can dramatically increase during the first 1-2 days after N fertilizer application and can take several weeks for the emission rate to drop to pre-fertilizer levels (Ludwig et al., 2001). Furthermore, the role of vegetation, acting as a net source of atmospheric NO_x when ambient NO_x concentration is below the "compensation point", while acting as a net sink of atmospheric NO_x when ambient NO_x concentrations are above it (Johansson, 1987; Thoene, Rennenberg & Weber, 1996; Slovik et al., 1996; Webber & Rennenberg, 1996). This significantly impacts the biotic NO_x emission inventory (Almaraz et al., 2018). Uncertainties also exist in the amount of NO_x emitted during the combustion of fossil fuels by vehicles and industry. According to Parrish (2006), the estimation of on-road vehicle NO_x emission has at least 10 to 15% uncertainty. For the mileage-based algorithm, which is used in the National Emission Inventory (NEI), the uncertainty is caused by the limited number of sites to determine the emission factors of vehicle classifications and emission types (Ingalls, 1989; Pierson et al., 1990; Fujita et al., 1992; Pierson et al., 1996; Singer and Harley, 1996). The uncertainty of the alternative fuel-based approach is caused by the fuel sales data and emission factors (Sawyer et al., 2000). The uncertainty in power plant NO_x emissions results from the choice of emission control technologies, of which the removal efficiencies of NO_x emission are different. NO_x removal by low NO_x burning, over-fire air reduction, and selective non-catalytic reduction is highly variable, ranging from 50 to 75% (Srivastava et al., 2005).

The nitrogen stable isotope composition of NO_x might be a useful tool to help resolve the uncertainties of how NO_x emission sources vary in space and time because natural and anthropogenic NO_x sources have distinctive $^{15}N/^{14}N$ ratios (Ammann et al., 1999; Felix et al., 2012; Felix and Elliott, 2013; Fibiger et al., 2014; Heaton, 1987; Hoering, 1957; Miller et al., 2017; Walters et al., 2015a, 2015b, 2018). This variability in NO_x $^{15}N/^{14}N$ ratios is quantified by

$$\delta^{15}N(NO_x)\ (‰) = [(^{15}NO_x/^{14}NO_x) / (^{15}N_2/^{14}N_2)_{air} - 1] \times 1000) \qquad \text{Eq. (1)}$$

Formatted: Font: Times New Roman, 12 pt

Formatted: Outline numbered + Level: 1 + Numbering Style: 1, 2, 3, … + Start at: 1 + Alignment: Left + Aligned at: 0" + Indent at: 0.25"

Deleted: ($NO_x = NO + NO_2$)

Deleted: .

Deleted: could be converted

Deleted:) in the atmospheric NO_x cycle.

Deleted: this process,

Deleted: concentration

Deleted: is

Deleted: S. E.,

Deleted: Due to its impacts on

Deleted: , and the environment

Deleted: is

Deleted: However

Deleted: a number of

Deleted: despite years of research. These include a). soil NO_x emissions caused by the application of N fertilizers (Shepherd, 1991; Ludwig et al., 2001; Galloway et al., 2004; Hudman, 2012; Houlton et al., 2013; Pilegaard, 2013) and

Deleted: (Johansson, 1987; Jacob & Wofsy, 1990; Hanson & Lindberg, 1991; Yienger & Levy II, 1995;

Deleted: ;

Deleted:); b). emissions from on-road vehicles estimated by different algorithms (

Deleted: &

Deleted: ; Cicero-Fernandez et al., 1997; Dreher & Harley, 1998; Dreher & Harley, 1998;

Deleted: ; Parrish, 2006); and c).

Deleted: due to

Deleted: implementation

Deleted: different NO_x

Deleted: (Felix et al., 2012;

Deleted: ; Xing et al., 2013

Deleted: Previous research has shown that there are distinctive differences in $\delta^{15}N$ values for NO_x from different emission sources (Fig. 1), such as soil (Li & Wang, 2008; Felix & Elliott, 2014; Yu & Elliott, 2017; Miller et al. … [1]

Moved down [1]: 1999; Pearson et al., 2000; Savard et

Deleted:), and power plants

Moved down [2]: (Heaton, 1987; Heaton, 1990; Snape,

Deleted: Walters et al, 2015a; Savard et al., 2017). … [2]

Moved (insertion) [3]

where $^{15}NO_x/^{14}NO_x$ is the measurement of relative abundance of ^{15}N to ^{14}N in atmospheric NO_x, compared with the ratios in air N_2 = 0.0036. Previous research has shown that there are distinctive differences in $\delta^{15}N$ values for NO_x from different emission sources and significant variations within each source (Fig. 1). Soil NO_x has the lowest $\delta^{15}N$ values (Li & Wang, 2008; Felix & Elliott, 2014; Yu & Elliott, 2017; Miller et al., 2018) followed by waste (Felix & Elliott, 2014) and NO_x emissions from vehicles (Moore, 1977; Heaton, 1990; Ammann et al., 1999; Pearson et al., 2000; Savard et al., 2009; Redling et al., 2013; Fibiger, 2014; Felix & Elliott, 2014; Walters et al., 2015a; Walters et al., 2015b). The NO_x emissions from natural gas power plants are isotopically heavier than soil and waste (Walters et al., 2015b) while those from coal-fired power plants have the highest values (Heaton, 1987; Heaton, 1990; Snape, 2003; Felix et al., 2012; Felix et al., 2015; Savard et al., 2017). The implement of emission control technology tends to increase NO_x $\delta^{15}N$ values in both coal-fired power plants (Felix et al., 2012) and vehicles (Walters et al, 2015a). These distinctive differences in $\delta^{15}N$ values among different NO_x emission sources suggest $\delta^{15}N$ could be an effective tracer of atmospheric NO_x sources. For example, Redling et al. (2003) found higher $\delta^{15}N$ of NO_2 in samples collected closer to the highway compared to those adjacent to a forest, showing the emissions from vehicles were dominant near the highway. A strong positive correlation between the amount of NO_x emission from coal-fired power plants within 400 km radial area of study sites and $\delta^{15}N(NO_3^-)$ of deposition has been demonstrated (Elliott et al., 2007; 2009). What is lacking is a systematic way of connecting $\delta^{15}N$ values of NO_x sources, regional emissions, and data from numerous studies that measure $\delta^{15}NO_y$ (Elliott et al., 2009; Garten, 1992; Hall et al., 2016; Occhipinti, 2008; Russell et al., 1998).

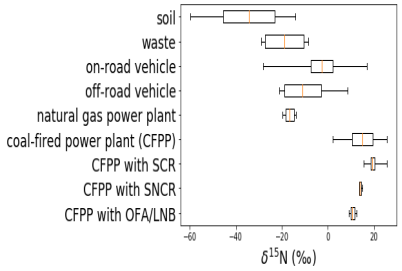

Figure 1: Box (lower quartile, median, upper quartile) and whisker (lower extreme, upper extreme) plot of the distribution of $\delta^{15}N$ values for various NO_x emission sources.

Here we have simulated the emission of $^{15}NO_x$ and its mixing in the atmosphere and compared the predicted $\delta^{15}N(NO_x, NO_3^-)$ values to observations. The $\delta^{15}N$ values of atmospheric NO_x are impacted by three main factors. The first is the inherent variability of the $\delta^{15}NO_x$ emissions in time and space. Secondly, atmospheric processes that mix the emitted NO_x, blurring multiple emission sources within a mixing lifetime relative to the NO_x chemical lifetime (2-7 hours), which depends on its concentration and photooxidation chemistry, that also vary in time and by location (Laughner & Cohen, 2019). And thirdly, isotope effects occurring during tropospheric photochemistry may alter the $\delta^{15}NO_x$ emissions as they are transformed from NO_x into NO_y. In this paper, we consider the effects from the first and second considerations, the temporal and spatial variation in NO_x

Moved (insertion) [4]

Moved (insertion) [1]

Moved (insertion) [2]

Deleted:

emission and the impacts from atmospheric transport and deposition processes (source and mixing hypothesis). We accomplish this by incorporating an input dataset of ^{15}N emissions used in simulations by the Chemistry-Transport Model (CTM) used in CMAQ (The Community Multiscale Air Quality Modeling System). In a companion paper, we will discuss the impacts of tropospheric photochemistry by incorporating a ^{15}N chemical mechanism (Fang et al., 2021) into CMAQ. The ultimate goal will be to evaluate the accuracy of the NO_x emission inventory using ^{15}N.

2. Methodology

2.1 Incorporating ^{15}N into NO_x emission datasets

The EPA trace gas emission model SMOKE (Sparse Matrix Operator Kernel Emissions) was used to simulate $^{14}NO_x$ and $^{15}NO_x$ emissions. $^{14}NO_x$ emissions were estimated using the SMOKE model based on the 2002 NEI (National Emission Inventory, USEPA, 2014), and ^{15}N emissions were determined using these $^{14}NO_x$ emissions and the corresponding $\delta^{15}N$ values of NO_x sources from previous research (Table 1). Using the definition of $\delta^{15}N$ (‰), $^{15}NO_x$ emitted by each SMOKE processing category (area, biogenic, mobile, and point) was calculated by

$$^{15}NO_x(i) = {}^{14}NO_x(i) \times {}^{15}R_{NO_x}(i) \qquad \text{Eq. (2)}$$

where $^{14}NO_x(i)$ are the NO_x emissions for each category (i) obtained from NEI and SMOKE and $^{15}R_{NOxi}$ is a ^{15}N emission factor ($^{15}NO_{Xi}/^{14}NO_{xi}$) calculated by:

$$^{15}R_{NO_x}(i) = \left(\frac{\delta^{15}N_{NO_x}(i)}{1000} + 1\right) \times 0.0036 \qquad \text{Eq. (3)}$$

$\delta^{15}N_{NOx(i)}$ is the $\delta^{15}N$ value of some NO_x source (i = area, biogenic, mobile, and point) and 0.0036 is the $^{15}N/^{14}N$ of air N_2, the reference point for $\delta^{15}N$ values.

Annual NO_x emissions for 2002 were obtained from the NEI at the county-level and were converted into hourly emissions on a 12 km x 12 km grid as previously published (Spak, Holloway, & Stone, 2007). The modeling domain includes latitudes between 37 º N and 45 º N, and longitudes between 98º W and 78º W, which fully covers the Midwestern US (Fig. 2, in yellow). SMOKE categorizes NO_x emissions into four "processing categories": Biogenic, Mobile, Point, and Area (Table 1). The choice of the 2002 version of NEI is, in part, arbitrary. However, to compare the model predicted $\delta^{15}N$ values with observations, it requires the emission inventory to be relevant to the same timeframe as the $\delta^{15}N$ measurements of the NO_y. The data sets we compare to the model (discussed below) span from 2002 to 2009, thus the 2002 inventory is more relevant than later inventories (2014 onward). The county-level annual $^{14}NO_x$ emission for the Midwestern US from NEI was converted to the dataset with hourly $^{14}NO_x$ emissions. Livestock waste and off-road vehicles classified as area sources and each county was gridded evenly. Power plants are regarded as the point source and are located in grids corresponding to their latitudes and longitudes. On-road vehicles were regarded as the mobile source by SMOKE estimated by MOBILE model (see SA). The soil NO_x produced by microbial nitrification and denitrification is classified as biogenic NO_x emission and was estimated by BEIS model (see SA).

Moved up [3]: where $^{15}NO_x/^{14}NO_x$ is the measurement of relative abundance of ^{15}N to ^{14}N in atmospheric NO_x, compared with the

Deleted: ratio of nitrogen in the air, which has a $^{15}N_2/^{14}N_2$ = 0.0036.
Here we have simulated the $\delta^{15}N$ values of atmospheric NO_x within the Midwestern United States, under different scenarios, and compared them with the recent measurements. The factors required to account for the processes that alter $\delta^{15}N$ of atmospheric NO_x during the NO_x chemical lifetime are: a). The variability of the $\delta^{15}N$ values of NO_x emissions in time and space; b). The transport and mixing of tropospheric NO_x by meteorology; c.) The wet and dry deposition of NO_x and NO_y; and d). The isotope effects occurring during the tropospheric photochemistry that transforms NO_x into NO_y. In a companion paper (Fang & Michalski, 2020), we discussed the effects due to the variation of the $\delta^{15}N$ value of different NO_x emission sources and their variation in time and space. In this previous ... [3]

Formatted: Font: Times New Roman, 12 pt

Formatted ... [4]

Deleted: In this study, we investigate the role ... [5]

Moved down [5]: 2, in yellow).

Deleted: A nested domain, which fully covers the st ... [6]

Deleted: in the NEI's are on-road gasoline, on-road ... [7]

Deleted: from NEI emission sectors

Deleted: previously discussed (Fang & Michalski, 2 ... [8]

Moved up [4]: 1).

Deleted: The

Deleted: based on the definition of $\delta^{15}N$ (‰).

Formatted: Font: Italic

Deleted: is

Formatted: Font: Italic

Formatted: Indent: First line: 4 ch

Deleted: each

Deleted: category

Formatted: Font: Italic

Deleted: (Table 1)

Deleted: natural abundance of ^{15}N (

Deleted: the

Deleted: thus $\delta^{15}N_{N2}$=0),

Deleted: measurements.

Moved (insertion) [5]

Deleted: $\delta^{15}N$

Deleted: total NO_x

Deleted: calculated

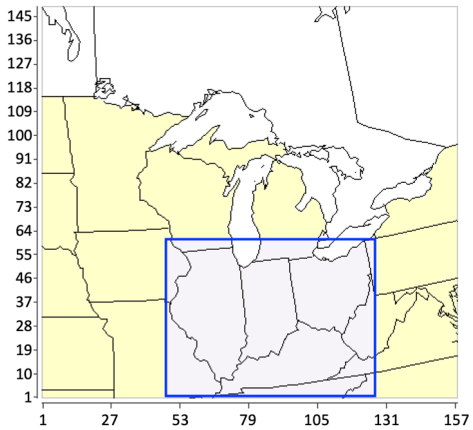

Figure 2: The full geographic domain (yellow) and extracted domain (light purple) for the study.

SMOKE Category	NEI Sector	δ^{15}N-NO_x (‰) range	δ^{15}N-NO_x (‰) this study
Biogenic	Soil	-59.8 ~ -14.0	-34.3 (Felix & Elliott, 2014)
Area	Livestock Waste	-29 ~ -8.5	-18.8 (Felix & Elliott, 2014)
	Off-road Gasoline	-21.1 ~ 8.5	-11.5 (Walters et al., 2015b)
	Off-road Diesel		-10.5 (Walters et al., 2015b)
Mobile	On-road Gasoline	-28.1 ~ 17	-2.7 (Walters et al., 2015b)
	On-road Diesel		-2.5 (Walters et al., 2015b)
Point	Coal-fired Fossil Fuel Combustion	-19.7 ~ 25.6	15 (Felix et al., 2012)
	Natural Gas Fossil Fuel Combustion		-16.5 (Walters et al., 2015)

Table 1: The δ^{15}N values (in ‰) for NO_x emission sources based on SMOKE processing category and NEI sector

2.1.1 Biogenic $^{15}NO_x$ emissions

The NO_x emission from the soil (Biogenic) was modeled in SMOKE using standard techniques (details in SA) and the δ^{15}N values of biogenic NO_x were taken from previous studies. Li & Wang (2008) measured the NO_x fluxes using dynamic flow chambers for 2 to 13 days after cropland soil was fertilized by either urea (n=9) or ammonium bicarbonate (n=9), and the δ^{15}N values of NO_x ranged from -48.9 ‰ to -19.8 ‰. Felix & Elliott (2014) used passive samplers to collect NO_2 in a cornfield for 20 days, before and after fertilizer application. The δ^{15}N values of

Moved down [6]: $\delta^{15}N_{NO_x\,(total)} = \left(\frac{{}^{15}NO_x\,(area)+{}^{15}NO_x\,(biog)+{}^{15}NO_x\,(mobile)+{}^{15}NO_x\,(point)}{{}^{14}NO_x\,(area)+{}^{14}NO_x\,(biog)+{}^{14}NO_x\,(mobile)+{}^{14}NO_x\,(point)} - 1\right) \times 1000$ Eq. (

Deleted: 4)
where

Moved down [7]: ${}^{15}NO_x\,(area) = \left(\frac{\delta^{15}N_{NO_x\,(waste)}}{1000} + 1\right) \times 0.0036 \times {}^{14}NO_x\,(waste)$

Moved down [8]: $+\left(\frac{\delta^{15}N_{NO_x\,(off-road\,gas)}}{1000} + 1\right) \times 0.0036 \times {}^{14}NO_x\,(off-road\,gas)$
$+\left(\frac{\delta^{15}N_{NO_x\,(off-road\,diesel)}}{1000} + 1\right) \times 0.0036 \times {}^{14}NO_x\,(off-road\,diesel)$ Eq. (5)

NO_x emissions from these measurements range from -30.8 ‰ to -26.5 ‰. Using a similar methodology, Miller et al. (2018) collected NO_2 between May and June finding $\delta^{15}N$ ranging from -44.2 ‰ to -14.0 ‰ (n=37). Yu & Elliott (2017) measured -59.8 ‰ to -23.4 ‰ in 15 samples from soil plots in a fallow field 2 weeks after the precipitation. Based on these studies we adopted an average $\delta^{15}N$ value for NO_x emissions from the soil of -34.3 ‰ (Li & Wang, 2008; Felix & Elliott, 2014; Yu & Elliott, 2017; Miller et al., 2018).

2.1.2 Mobile $^{15}NO_x$ emissions

The SMOKE NO_x emission from on-road vehicles used standard methods (details in SA) and used $\delta^{15}N$ values from prior studies (Moore, 1977; Heaton, 1990; Ammann et al., 1999; Pearson et al., 2000; Savard et al., 2009; Redling et al., 2013; Felix & Elliott, 2014; Fibiger, 2014; Walters et al., 2015a, 2015b). We have excluded studies that infer NO_x $\delta^{15}N$ by measuring plant proxies or passive sampling in the environment (Ammann et al., 1999; Pearson et al.,2000; Savard et al. 2009; Redling et al., 2013; Felix & Elliott, 2014). This is because of equilibrium and kinetic isotope effects that can occur as NO_x reacts in the atmosphere to form NO_y, prior to NO_x deposition. In addition, the role vegetation plays in NO_x removal and atmospheric processes that mix the $\delta^{15}N$ of emission with the surroundings can also alter the $\delta^{15}N$ from the mobile source. Instead, we estimated the $\delta^{15}N$ value of NO_x emissions from vehicles only using studies that directly measured tailpipe NO_x emissions. Moore (1977) and Heaton (1990) collected tailpipe NO_x spanning -13 ‰ to 2 ‰, with an average of -7.5 ± 4.7 ‰. Neither Heaton nor Moore noted whether these 6 vehicles were equipped with any catalytic NO_x reduction technology, but it is unlikely since the late 1970 and 80's s vehicles were seldomly equipped with catalytic NO_x reduction technology. Fibiger (2014) measured 5 samples of NO_x from diesel engines without SCR emitted into a smog chamber, the $\delta^{15}N$ values range from -19.2 ‰ to -16.7 ‰ (±0.97 ‰). The most comprehensive studies on vehicle NO_x $\delta^{15}N$ values are by Walters et al. (2015a, 2015 b) who measured gas and diesel vehicles separately, including those with and without three-way catalytic converter (TCC) and SCR technology. They also measured on-road and off-road vehicles separately. This research showed that the $\delta^{15}N$ of NO_x for vehicles without SCR or when SCR was not functioning was negative, at around -15‰. As SCRs warmed and became efficient at reducing NO_x the $\delta^{15}N$ value became less negative and even went positive. The measurements showed that the $\delta^{15}N$ values of NO_x emitted by gasoline on-road vehicles averages at -2.5 ± 1.5 ‰, and on-road diesel ranged from -5 ‰ to 0 ‰.

The emission rate of $^{15}NO_x$ from the mobile source was determined by Eq. 4 grid by grid, according to the contributions from on-road gasoline vehicles and on-road diesel vehicles, as well as their corresponding $\delta^{15}N$ values of these two types of vehicles grid by grid. NO_x emissions from off-road vehicles are regarded as area sources in SMOKE, which were processed over each county. In contrast, NO_x emissions from on-road vehicles are regarded as the mobile source in SMOKE, which will be processed along each highway. Each grid emission rate of $^{15}NO_x$ was assigned based on the contributions from gasoline and diesel vehicles, as well as the relative $\delta^{15}N$ values. The $\delta^{15}N$ of on-road gasoline vehicles (-2.7 ± 0.8 ‰) was based on the average of the vehicle travel time within each region with the same zip code (Walters et al., 2015b).

$$^{15}NO_x\,(mobile) = \left(\frac{\delta^{15}N_{NO_x\,(on-road\,gas)}}{1000} + 1\right) \times 0.0036 \times {}^{14}NO_x\,(on-road\,gas) + \left(\frac{\delta^{15}N_{NO_x\,(on-road\,diesel)}}{1000} + 1\right) \times 0.0036 \times {}^{14}NO_x\,(on-road\,diesel) \quad \text{Eq. (4)}$$

Where $\delta^{15}N_{NO_x\,(on-road\,gas)} = -12.35 + 3.02 \times \ln(t + 0.455)$

Deleted: 6

Deleted: where

Formatted: Indent: First line: 4.5 ch

2.1.3 Point source $^{15}NO_x$ emissions

NO_x point sources are large anthropogenic NO_x emitters located at a fixed, stationary position such as EGUs (electric generating units). Fugitive dust does not significantly contribute to point NO_x emissions, so our inventory focused only on power plants (Houyoux, 2005). Power plants were separated into two different types: EGU and Non-EGU (e.g. commercial and industrial combustions). The $\delta^{15}N$ value of NO_x emitted from power plants have been estimated to vary from -19.7 ‰ to 25.6 ‰ (Heaton, 1987; Heaton, 1990; Snape, 2003; Felix et al., 2012; Felix et al., 2015; Walters et al., 2015b; Savard et al., 2017). We have ignored studies that measured $\delta^{15}N$ of NO_3^- or HNO_3 from EGUs (Felix et al., 2015, Savard et al., 2017) and instead, only consider those studies that directly measured $\delta^{15}N$ of NO_x. Heaton (1990) collected 5 samples from the different coal-fired power stations finding NO_x from 6 ‰ to 13 ‰, with a standard deviation of 2.9 ‰. Snape (2003) measured $\delta^{15}N$ values of 36 samples from power plants using three different types of coals in combustion chars in a drop tube reactor, with values ranging from 2.1 ‰ to 7.2 ‰, with a standard deviation of 1.37 ‰. The most comprehensive study on coal-fired power plants' NO_x values was by Felix et al. (2012). They measured the $\delta^{15}N$ values of NO_x emission from the coal-fired power stations with and without different emission control technologies. 16 coal-fired power plants with SCR, 3 coal-fired power plants with SNCR, 15 coal-fired power plants with OFA/LNB, and 8 coal-fired power plants without emission control technology were measured. The $\delta^{15}N$ values of NO_x emissions from these 42 measurements range from 9 ‰ to 25.6 ‰, with a standard deviation of 4.51 ‰. The NO_x $\delta^{15}N$ values when different emission control technologies were used varied: the $\delta^{15}N$ values of NO_x emissions from coal-fired power plants with SCR range from 15.5 ‰ to 25.6 ‰, those with SNCR ranged from 13.6 ‰ to 15.1 ‰, and those with OFA/LNB ranged from 9.0 ‰ to 12.6 ‰. The $\delta^{15}N$ values of NO_x emissions from coal-fired power plants without emission control technology range from 9.6 ‰ to 11.7 ‰, with a standard deviation of 0.79 ‰. According to Xing et al. (2013), about half of the coal-fired power plants in the United States are equipped with SCR. Thus, we assume 15 ‰ for the NO_x emissions from coal-fired power plants, which is the average between SCR and other emission control technologies.

The most comprehensive study on natural gas-fired NO_x values (Walters et al. 2015) collected 12 flue samples on the rooftop of a house from the ventilation pipe of a natural gas low-NO_x burner residential furnace without NO_x emission control technology. The measurement showed that the $\delta^{15}N$ values of NO_x emitted by natural gas power plants average -16.5 ± 1.7 ‰, which we used for the NO_x emission from natural gas power plants. The reason for using these values is because they were measurements taken directly from the exhaust pipes, rather than inferring from downwind area or from rain samples, emitted by natural gas power plants, and included power plants with and without SCR technology. The latitude, longitude, and point sources characteristics (EGU and non-EGU, coal-fired or natural gas-fired, implementation of emission control technology) of each power plant was obtained from the US Energy Information Administration (2017). The power plants were assigned grids by their latitudes and longitudes, and the $\delta^{15}N$ values were assigned to these grids based on their emission characteristics, before determining the emission rate of $^{15}NO_x$ from point source using Eq. (2) and (3).

2.1.4 Area source $^{15}NO_x$ emissions

Area NO_x (details in SA) $\delta^{15}N$ values were based on the assumption that livestock waste and off-road vehicles (utility vehicles for agricultural and residential purposes) accounted for total area sources. Livestock waste NO_x $\delta^{15}N$ values were taken from Felix & Elliott (2014) since it is currently the only study about the $\delta^{15}N$ value of NO_x livestock waste emissions. They placed a

passive sampler with ventilation fans in an open-air and closed room in barns of cows and turkeys, respectively. The $\delta^{15}N$ values of NO_x emissions from these measurements range from -29 ‰ to -8.5 ‰. Among these samples, the $\delta^{15}N$ of NO_x emissions from turkey waste averages at -8.5 ‰, the $\delta^{15}N$ of NO_x emissions from cow waste averages at -24.7 ‰. We used -18.8 ‰ as the values of $\delta^{15}N$ values for NO_x emissions from livestock waste, which is the weighted average of the $\delta^{15}N$ of NO_x from turkey waste and cow waste emissions. We used the $\delta^{15}N$ values from Walters et al. (2015b) to estimate the $\delta^{15}N$ value of NO_x emissions from the off-road vehicle since it is the latest in-depth study that measured the $\delta^{15}N$ value of NO_x specifically from the off-road vehicle. They collected 45 samples from the tailpipe of 9 different off-road vehicles (gasoline and diesel) with and without SCR, and before and after the sufficient engine warm-up times. The measurement showed that the $\delta^{15}N$ values of NO_x emitted by gasoline-powered off-road vehicles averaged -11.5 ± 2.7 ‰, diesel off-road vehicles without SCR averaged -19 ‰ ± 2 ‰, and diesel off-road vehicles with SCR averaged -2 ‰ ± 8 ‰. The emission rate of $^{15}NO_x$ from area source was determined by Eq. 5 grid by grid, according to the contributions from waste, off-road gasoline vehicle, and off-road diesel vehicle, as well as their corresponding $\delta^{15}N$ values based on previous researches.

$$^{15}NO_x\,(area) = \left(\frac{\delta^{15}N_{NO_x\,(waste)}}{1000} + 1\right) \times 0.0036 \times {}^{14}NO_x\,(waste) + \left(\frac{\delta^{15}N_{NO_x\,(off-road\ gas)}}{1000} + 1\right) \times 0.0036 \times {}^{14}NO_x\,(off-road\ gas) + \left(\frac{\delta^{15}N_{NO_x\,(off-road\ diesel)}}{1000} + 1\right) \times 0.0036 \times {}^{14}NO_x\,(off-road\ diesel) \quad \text{Eq. (5)}$$

Moved (insertion) [7]

Moved (insertion) [8]

The $^{15}NO_x$ emission data files of each SMOKE processing category was incorporated into the final dataset based on the $\delta^{15}N$ values from previous research (Table 1) and Eq. (2-5).

$$\delta^{15}N_{NO_x\,(total)} = \left(\frac{\frac{^{15}NO_x\,(area) + {}^{15}NO_x\,(biog) + {}^{15}NO_x\,(mobile) + {}^{15}NO_x\,(point)}{^{14}NO_x\,(area) + {}^{14}NO_x\,(biog) + {}^{14}NO_x\,(mobile) + {}^{14}NO_x\,(point)}}{0.0036} - 1\right) \times 1000 \quad \text{Eq. (6)}$$

Moved (insertion) [6]

2.2 Simulating atmospheric $\delta^{15}N(NO_x)$ in CMAQ

In order to investigate the role of mixing in the spatiotemporal distribution of NO_x $\delta^{15}N$ values, CMAQ was used to simulate the meteorological transport effects (advection, eddy diffusion, etc). In this "emission + mixing" scenario grid specific NO_x $\delta^{15}N$ values emitted blur as NO_x mixes across the regional scale. This blurring will depend on grid emission strength and mixing vigor and is effectively treating NO_x as a conservative tracer. The simulations used the 2002 National Emission Inventory (NEI), as well as 2002 and 2016 meteorological conditions respectively, in order to explore how meteorological conditions will impact the atmospheric $\delta^{15}N(NO_x)$. Simulations covering the full domain and extracted domain were conducted, in order to explore and eliminate the bias near the domain boundary.

In addition, CMAQ simulated the $\delta^{15}NO_x$ effect by NO_x removal using enhanced deposition. These "emission + mixing + enhanced deposition" simulations were **not** imposing an isotope effect related to dry/wet deposition, rather they are an attempt to show how "lifetime chemistry" alters NO_x $\delta^{15}N$ values by removing NO_x before it can be transported significant distances. For example, in an "emission + mixing" scenario NO_x from a high emission powerplant could travel across the domain altering regional NO_x $\delta^{15}N$ as it mixes with other grids. By contrast, in the "emission + mixing + enhanced deposition" scenario most of that NO_x would be removed near the power plant,

effectively constricting its $\delta^{15}N$ influence. This enhanced deposition effect was simulated by disabling the chemistry module in CMAQ and enhancing the NO_x dry deposition rates (discussed in 2.2.3). This has an added advantage in that the deposited NO_x $\delta^{15}N$ should be similar to the NO_3^- $\delta^{15}N$, which is not being generated in this model. We emphasize that in this model the isotope effects associated with the photochemical transformation of NO_x into HNO_3 (and other higher N oxides) and deposition are ignored and will be addressed in the forthcoming paper.

2.2.1 Meteorology input dataset

To explore the impact of atmospheric processes, the meteorology input datasets for the years 2002 and 2016 were prepared and compared. The CMAQ CTM (CCTM) used the NARR (North American Regional Reanalysis) and NAM (North American Mesoscale Forecast System) to convert the weather observations (every 3 hours for NARR, every 6 hours for NAM Analyses) into gridded meteorological elements, such as temperature, wind field, and precipitation, with the horizontal resolution of 12 km, and 34 vertical layers, with the thickness, increases with height, from 50 m near the surface to 600 m near the 50 mb pressure level. These were used to generate the gridded meteorology files on an hourly basis, using the Weather Research and Forecasting Model (WRF). To maintain consistency between the NO_x emission dataset and the meteorology, the same coordinate system, spatial domain, and grid size used in the SMOKE model were used in the WRF simulation. The WRF outputs were used to prepare the CMAQ-ready meteorology input dataset using CMAQ's MCIP (the Meteorology-Chemistry Interface Processor; see SA for details). In these emission-only simulations, the deposition of NO_x was effectively set to zero. This was accomplished by defining YO $=^{14}NO$ and $YO_2 = {}^{14}NO_2$ (in addition to ZO $=^{15}NO$ and $ZO_2 = {}^{15}NO_2$) and setting their VDs (deposition velocities) to 0.001 (since setting them to zero collapses the simulation) in the namelist for the gas-phase species (GC_cb6r3_ae6_aq.nml).

2.2.2 Initial condition and boundary condition for the simulation

The meteorological fields generated by MCIP were used as the inputs for Initial Conditions Processor (ICON) and Boundary Conditions Processor (BCON), used for running CCTM of CMAQ. The ICON program prepares the initial chemical/isotopic concentrations in each of the 3D grid cells for use in the initial time step of the CCTM simulation. The BCON program prepares the chemical/isotopic boundary condition throughout the CCTM simulation. The CMAQ default ICON and BCON for a clean atmosphere were used, which had $NO_x < 0.25$ ppb. The $^{15}NO_x$ were added to the outputs of ICON and BCON, with the concentration equal to $0.0036[^{14}NO_x]$, which assumes $\delta^{15}N = 0$ at the initial time step and outside the domain of the simulation.

2.2.3 The role of deposition and chemical transformation of NO_x

The deposition rates $^{14}NO_x$ and $^{15}NO_x$ were varied to assess their role in the spatiotemporal distribution of NO_x $\delta^{15}N$ value and to emulate photooxidation of NO_x. In these "emission + mixing + enhanced deposition" simulations, the molecular mass of Y and Z were set equal (14) to ensure no isotope effect was induced by dry deposition, since the equations for dry deposition have a mass term in the diffusion coefficient calculation. The $^{15}NO_x/NO_x$ deposition rates were amplified by first magnifying it to 20 times normal (14 kg/hectare/yr) and testing for the change in NO_x concentration relative to the normal deposition rate. Multiple tuning trials were conducted until the e-folding time (lifetime) of NO_x in the atmosphere across the domain averaged about 1 day. This is a typical average NO_x lifetime for a combination of urban, suburban, and rural environments (Laughner & Cohen, 2019). This approach is limited since NO_x lifetime varies

Formatted: Font: 12 pt

Formatted: Normal, No bullets or numbering

Deleted: year

Deleted: preparation of the meteorology input datasets for the simulation using

Deleted: requires multiple steps. The first step is to generate the input for the CTM meteorological model using

Deleted:). Both NARR and NAM Analyses are regional weather model datasets covering North America and were obtained from the National Centers for Environmental Information (2019). NARR and NAM were used

Deleted: The simulation years were 2002 and 2016 and were selected based on the same timeframe as selected NO_y $\delta^{15}N$ measurements. These include measurements of $\delta^{15}N(NO_3^-)$ at 8 NADP (National Atmospheric Deposition Program) sites within Indiana, Illinois, Ohio, and Kentucky in 2001-03, and the direct measurements of $\delta^{15}N(NO_x)$ between July and August 2016 (Mase, 2010; Riha, 2013). ¶ The second step was

Deleted:) using the input files prepared by the NARR and NAM analyses.

Deleted: The same as the emission dataset, the projection type of WRF output is Lambert Conformal, with the standard parallel of 33 N and 45 N, the central meridian of 97 W. The output dataset of WRF has the same spatial domain as the emission dataset with a size of 12 km.

Deleted: The last step is to prepare the CMAQ-ready meteorology input dataset based on WRF outputs, by running MCIP (the Meteorology-Chemistry Interface Processor), one of the major components of CMAQ. The MCIP first obtains the necessary parameters (Table S1) from WRF outputs. Then the MCIP extracts the data of the necessary parameters for the appropriate geographic domain, which are slightly smaller than the domain of WRF outputs since the cells near the boundary are inadequate for CMAQ simulation. For example, the geographic domain of WRF outputs for this research is 160 grids in the east-west direction and 151 grids in the north-south direction. Therefore, MCIP extracts the WRF outputs into 157 g ... [9]

Formatted: Normal, No bullets or numbering

Formatted: Font: 12 pt

Deleted: For this study, the initial condition was derived from the ASCII vertical profiles to create a "clean" ... [10]

Deleted: for

Deleted: Similarly, the boundary condition was derived from the ASCII vertical profiles for this study,

Deleted: assume a "clean" atmospheric chemical condition (NO_x concentration lower than 0.25 ppb at surface layer)

Deleted: .

Formatted: Font color: Black

Deleted: The $^{14}NO_x$ in the outputs of ICON and BCON were replicated and set as nonreactive chemical. The ... [11]

depending on oxidation capacity, with urban NO_x lifetimes (~2-11 hours) being significantly shorter than in rural conditions (Fang et al., 2021). This limitation will be resolved once ^{15}N is included in the gas and aerosol chemistry modules to future versions of CMAQ.

2.2.4 The simulation over the extracted domain

As mentioned in section 2.2.4, atmospheric NO_x $\delta^{15}N$ = 0‰ for initial condition and boundary condition. As a result, the bias occurs near the border of the research area, mainly under the following two circumstances. Firstly, when the air mass transports out of the research area (Fig. S1). Due to the lack of the emission dataset, Canada is considered an "emission-free zone" for this research. As a result, the atmospheric NO_x is diluted, which impacts its $\delta^{15}N$ values, especially for those with extreme $\delta^{15}N$ values ($\delta^{15}N$ < -15‰ or $\delta^{15}N$ > 5‰). Secondly, the air mass with $\delta^{15}N(NO_x)$ = 0 transports from the "emission-free zone" to the research area (Fig. S2), the atmospheric $\delta^{15}N(NO_x)$ is flattened. Therefore, to avoid the bias near the border, the extracted domain that only covers Indiana, Illinois, Ohio, and Kentucky was determined (Fig. 2, in light purple), where the measurements of $\delta^{15}N$ values at NADP sites are available (Mase, 2010; Riha, 2013). The boundary condition for the simulation over the extracted domain is based on the CCTM output of the full-domain simulation (BCON code available on Zenodo.org (10.5281/zenodo.4311986)).

Results and Discussion

3.1 Simulated spatial variability of NO_x emission rates

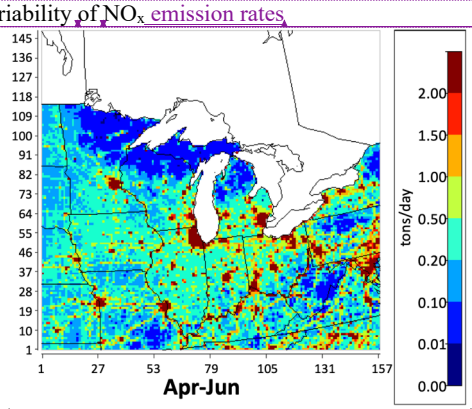

Figure 3: Total NO_x emission in the Midwest between April and June in tons/day. High NO_x emissions are associated with major urban areas such as Chicago, Detroit, Minneapolis-St Paul, Kansas City, St. Louis, Indianapolis, and Louisville.

We first examine the spatial heterogeneity of the NO_x emission rate for a single time period to illustrate the overall pattern of NO_x emission over the domain (Fig. 3). This is because the $\delta^{15}N$ value of total NO_x emission is determined by the fraction of each NO_x source (Eq. 6), which in turn is a function of their emission rates. Since our NO_x emissions are gridded by SMOKE using

Deleted: 5….4, atmospheric NO_x $\delta^{15}N$ = 0‰ for initial condition and boundary condition. As a result, the bias occurs near the border of the research area, mainly under the following two circumstances: a). When… Firstly, when the air mass transports out of the research area (Fig. S1) ... [12]

Deleted: Column Break

Formatted: Font: Times New Roman, 12 pt

Deleted: ¶

Deleted: atmospheric

Formatted ... [13]

Deleted: in $\delta^{15}N$

Formatted: Font: Times New Roman, 12 pt

Formatted ... [14]

Deleted: ... [15]

Deleted: $\delta^{15}N$ values at …mission rate for a specific…ingle time within the Midwestern domain and explore how atmospheric processes alter…eriod to illustrate the $\delta^{15}N$ values relative to …verall pattern of NO_x emission over the "no transport" simulation. ... [16]

the NEI, they are, by definition, corrected with respect to the NEI. However, a brief discussion of the salient geographic distribution of NO_x emissions and comparisons with other studies is warranted for completeness and as a backdrop for the discussion of NO_x fractions and resulting $\delta^{15}N$ values. We have arbitrarily chosen to sum the NO_x emissions during the April to June time period for this discussion (Fig. 3).

The seasonal average NO_x emissions within the geographic domain during April to June range from less than 0.01 tons N/day to more than 15 tons N/day, with the seasonal grid average of 0.904 tons/day. This average agrees well with estimates in previous studies for the United States, which were between 0.81 and 1.02 tons/day (Dignon & Hameed, 1989; Farrell et al., 1999; Selden et al., 1999; Xing et al, 2012). Within 75% of the geographic domain, the NO_x emissions are relatively low, ranging from between 0 and 0.5 tons/day (Fig. S3). Geographically, these grids are located in rural areas some distance away from metropolitan areas and highways (Fig. 3). NO_x emissions within about 20% of the grids is relatively moderate, ranging between 0.5 and 2.0 tons/day (Fig. S3). Geographically, these grids are mainly located along major highways and areas with medium population densities (Fig. 3). Urban centers comprise about 5% of the grids within the geographic domain and these have high NO_x emissions rates, ranging between 2.0 and 15.0 tons/day (Fig. S3). The metropolitan area's average is 5.03 tons/day, which is nearly 14 times of the average emission rate over the rest of the grids within the geographic domain (0.37 tons/day) due to the high vehicle density associated with high population densities. The highest emissions rates are located within large cities (Fig. 3), such as Chicago, Detroit, Minneapolis-St Paul, Kansas City, St. Louis, Indianapolis, and Louisville, as well as the edge of the east coast metropolitan area (dark red). Summing the NO_x emissions among the grids that encompass these major midwestern cities, yields city-level NO_x emission rates that vary from 61.2 tons/day (Louisville, KY) to 634.1 tons/day (Chicago, IL). These city-level NO_x emission rates (Table S4) agree well with estimates derived from the Ozone Monitoring Instrument (Lu et al., 2015). Grids containing power plants are the significant NO_x hotspots within the geographic domain. These account for less than 1% of the grids, but the NO_x emissions from a single grid that contains a power plant can be as high as 93.4 tons/day. Geographically, the power plants are mainly located along the Ohio River valley, near other water bodies, and often close to metropolitan areas (Fig. 3). The NO_x emission rates of the major power plants within the Midwest simulated by SMOKE (Table S5) match well with the measurement from the Continuous Emission Monitoring System (CEMS) (de Foy et al., 2015; Duncan et al., 2013; Kim et al., 2009). The geographic distribution of grid-level annual NO_x emission density in our simulation also agrees with the county-level annual NO_x emission density discussed in the 2002 NEI booklet (Fig. S4; USEPA, 2018b).

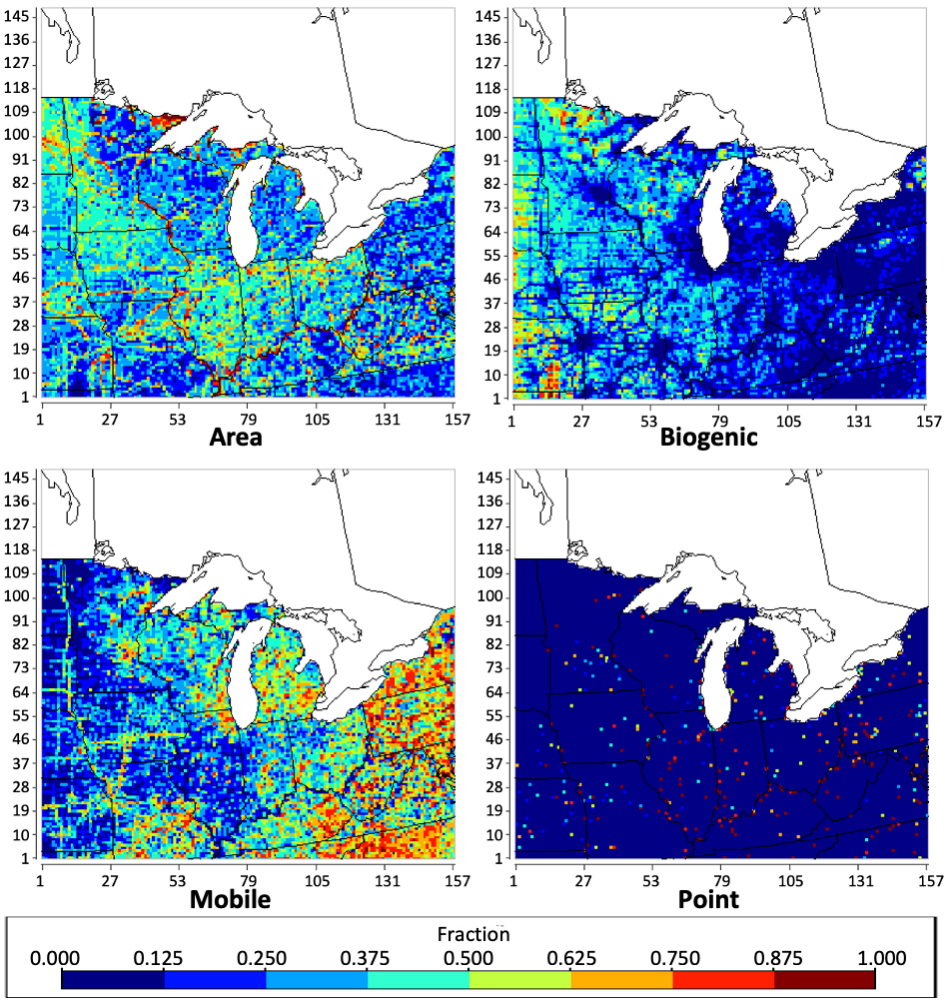

Figure 4: The geographical distribution of the fraction of NO_x emission from each SMOKE processing category (area, biogenic, mobile, point) over each grid throughout the Midwest between April and June based on NEI-2002.

Moved (insertion) [9]

Formatted: Font: 12 pt

Formatted: Normal, Indent: First line: 2 ch, No bullets or numbering

We next examine the spatial heterogeneity of the NO_x source fractions (Fig. 4) for the same time period (April to June). The NO_x fraction (f) is defined as the amount of NO_x from a source category normalized to total NO_x (f_s =NO_x(source)/NO_x(total). Since the $\delta^{15}NO_x$ is determined by the NO_x emission fractions within each grid it is important to understand where in the domain these fractions differ and why. The area sources, which mainly consist of off-road vehicles, agriculture production, residential combustion, as well as the industrial processes, which are individually too low in magnitude to report as point sources, are fairly uniform in their distribution across the domain.

The SMOKE simulation shows that NO_x emissions from area sources contribute an average NO_x emission fraction (f_{area}) of 0.271 for total NO_x emission and 0.290 for anthropogenic NO_x emission within the Midwest from April to June. The fractions of NO_x emission from area sources show a clear spatial variation and range from 0.125 to 0.5 over about 75% of the grids (Fig. S5). Geographically, the grids with relatively higher f_{area} are located in the rural area away from highways, especially in the states of Indiana, Illinois, Iowa, Minnesota, and Ohio, where agricultural is the most common land use classification. In the states of Wisconsin and Missouri, the f_{area} is slightly lower due to the higher fraction of NO_x emission from biogenic sources (f_{biog}). In the states of Pennsylvania and Michigan, the f_{area} is slightly lower due to the higher fraction of NO_x emission from mobile sources (f_{mobile}). In addition, the grids with f_{area} greater than 0.75 are mainly located along the Mississippi River and Ohio River, due to wastewater discharge.

The fraction of biogenic NO_x (f_{biog}) that are predominately by-products of microbial nitrification and denitrification occurring in soil, shows the clear spatial variation and is highest (from April to June) in the western portion of the domain (Fig. 4). The average fraction of biogenic NO_x emission within the Midwest from April to June and is 0.065, which is less than 0.5 in more than 90% of the grids within the geographic domain (Fig. S5). Geographically, the grids with relatively high f_{biog} are located in the western regions of the Midwest, away from cities and highways, in the states of Minnesota, Iowa, Missouri, Wisconsin, and Illinois, where the density of agricultural acreage and natural vegetation is higher than other states. Furthermore, within regions with higher f_{biog}, the obvious low f_{biog} values occur in the megacities and along the highways, which agrees well with the land-use related to the biogenic emission.

The SMOKE simulation shows that the NO_x emissions from mobile sources contribute to the fraction (f_{mobile}) of 0.325 for total NO_x emission and 0.347 for anthropogenic NO_x emission within the Midwest from April to June. The f_{mobile} shows a clear spatial variation, with relatively higher f_{mobile} are located in major metropolitan regions and along the highways, where vehicles have the highest density. In addition, within the states with lower f_{mobile}, the obvious high f_{mobile} values occur in the megacities and along the highways, which agrees well with the vehicle activities (US Census Bureau, n.d.). The value of f_{mobile} within the geographic domain distributes evenly on the histogram (Fig. S5).

The point sources consist mainly of EGUs, as well as commercial and industrial processes involving combustion. Based on the SMOKE simulation, the NO_x emission from point sources contributes to the fraction (f_{point}) of 0.339 for total NO_x emission and 0.363 for anthropogenic NO_x emission within the Midwest from April to June. The fractions of NO_x emission from the point source over each grid cell within the geographic domain show a clear spatial variation. Geographically, the NO_x emission from point sources is dominant at the grids, where the power plants are located, mainly along the Ohio River valley and near other water bodies close to metropolitan areas. The point sources have no contribution to the NO_x emission among about 96% of the grids within the geographic domain. The rest of the 4% of the grids within the geographic

Deleted: "no transport

domain are the locations of power plants. About 1/4 of the power plants are not at the same grids as highways, thus these grids have a fraction of at least 0.9 NO_x emission from point sources. Whereas the other 3/4 of the power plants share the same grids with highways/cities, thus the point sources become relatively less dominant, due to the dilution by the NO_x emission from mobile sources.

3.2 Simulated spatial variability in $\delta^{15}NO_x$

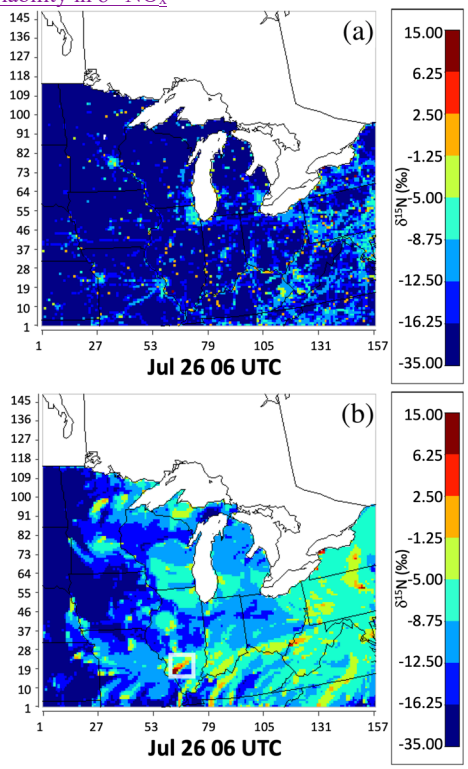

Figure 5: The $\delta^{15}N$ values of NO_x emission, (a: "no transport" scenario) and the $\delta^{15}N$ values of atmospheric NO_x based on NEI-2002 and 2016 meteorology (b: "with transport" scenario), at 06 UTC on July 26, are presented by color in each grid. The warmer the color, the higher $\delta^{15}N$ values of atmospheric NO_x.

Using these NO_x emission source fractions in each grid, the $\delta^{15}N$ values of NO_x were simulated. Here, the spatial heterogeneity of $\delta^{15}N$ values of NO_x for a single time period is discussed. The "emission only" simulation of NO_x $\delta^{15}N$ values (at 06 UTC on July 26) ranged

Formatted: Indent: First line: 2 ch

Deleted: shows that the domain grids

from -34.3‰ to 14.9‰ (Fig. 5a). The majority of the grids within the domain have NO_x $\delta^{15}N$ values lower than -16.3‰. These low $\delta^{15}N$ values across most of the domain are due to the $\delta^{15}N$ of -34.3‰ for biogenic NO_x emission sources in sparsely populated areas where intensive agriculture dominates the land use (Fig. 5a). The NO_x $\delta^{15}N$ values for grids within big cities mainly ranged between -8.75‰ and -5‰ due to the higher fraction of NO_x emission from on-road vehicles ($\delta^{15}N$ = -2.7 ± 0.8‰), which also resolve major highways. The highest value of $\delta^{15}N$ occurs at the grids, where the coal-fired EGUs (+15‰) and hybrid-fired EGUs are the dominant NO_x source (Fig. 5a).

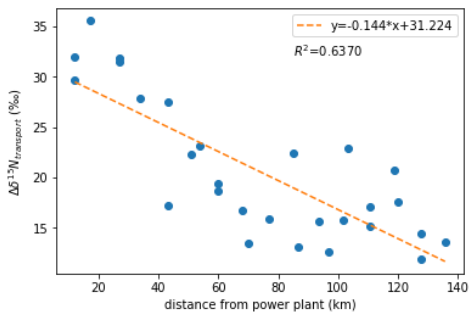

Figure 6: The $\Delta\delta^{15}N_{transport}$ along the plume (colored in dark red to orange inside the white box on Fig. 5b) over the distance from the power plant Baldwin Energy Complex (located at southwestern border of Illinois).

The effect of atmospheric mixing on the $\delta^{15}NO_x$ spatial distribution was then taken into account by coupling the $^{15}NO_x$ emissions to the meteorology simulation. There are significant differences between $\delta^{15}NO_x$ values in the "emission only" (Fig. 5a) and the "emission + transport" (Fig. 5b) simulations. For example, under the "emission only" scenario (Fig. 5a) the map of $\delta^{15}NO_x$ values clearly shows the locations of big cities, major highways, and power plants, but these features are much less obvious in the "emission + transport" (Fig. 5b) simulations. The isotopically heavier NO_x emission from big cities disperses to the surrounding rural areas so that the $\delta^{15}NO_x$ values in rural areas become elevated relative to the emission-only simulation. Similarly, the NO_x emitted along major highways is transported to the surrounding grids, so that the atmospheric NO_x at the grids around the major highways becomes isotopically heavier relative to the "emission only" scenario. We define $\Delta\delta^{15}N_{transport}$ as the $\delta^{15}N$ difference between "emission only" and "emission + transport" scenarios within the grids covered by the plume to quantify this effect (Fig. 6). The most obvious and interesting example is the influence of grids containing coal-fired EGUs on the surrounding region. For example, the southern Illinois' Baldwin Energy Complex (marked with a transparent white box on Fig. 5b) that uses subbituminous coal and bituminous coal as its major energy source. The $\Delta\delta^{15}N_{transport}$ in the regions is altered as a function of distance away from the EGU. In this time snapshot (06 UTC on Jul 26), the northeastwards propagating plume of NO_x emission from the EGU creates higher $\delta^{15}NO_x$ over 135 km away (Fig. 6). The domain average $\delta^{15}N$ increases from -20.2‰ under the "emission only" scenario to -11.5‰ under the "emission +

Moved (insertion) [10]

Deleted: Figure 3a).

Moved up [10]: The majority of the grids within the domain have NO_x $\delta^{15}N$ values lower than -16.3‰.

Deleted: (nitrification and denitrification) …n sparsely populated areas where intensive agriculture dominates the land use (Fig. 3a…a). The NO_x $\delta^{15}N$ values of NO_x emitted into…or grids within big cities mainly ranged between -8.75‰ and -5‰. This is… due to the higher fraction of NO_x emission from on-road vehicles having a …$\delta^{15}N$ of… -2.7 ± 0.8‰. The fraction of NO_x emission from on-road vehicles at the grids…), which also resolve major highways is relatively lower, comparing to the grids within big cities, while still higher than most of the grids within the domain. Thus, the $\delta^{15}N$ values along the major highways ranged between -16.25‰ and -8.75‰. ... [17]

Formatted: Font color: Auto

Deleted: (using both coal and natural gas (-16.5‰) for combustion) are dominant, showing gold (-1.25‰ ~ +2.5‰) and red/dark red (+2.50‰ and above) on the map (Fig. 3a

Formatted: Font color: Text 1

Deleted: and transport …n the NO_x $\delta^{15}N$…$^{15}NO_x$ spatial distribution were…as then taken into account by coupling $^{15}NO_x$ emissions (Fang & Michalski, 2020) …o the meteorology simulation. There are significant differences between $\delta^{15}N(NO_x)$…$^{5}NO_x$ values in the "no transport…mission only" (Fig. 3a…a) and the "with…mission + transport" (Fig. 3b…b) simulations. For example, under the "no transport…mission only" scenario (Fig. 3a…a) the map of $\delta^{15}N(NO_x)$…$^{5}NO_x$ values clearly shows the locations of big cities, major highways, and power plants, but these features are much less obvious in the "with…mission + transport" (Fig. 3b…b) simulations. The isotopically heavier NO_x emission from big cities, such as Chicago, Detroit, Minneapolis-St Paul, Kansas City, St. Louis, Indianapolis, and Louisville,…disperses to the surrounding rural areas so that the $\delta^{15}N(NO_x)$…$^{5}NO_x$ values in rural areas are…ecome elevated relative to values similar to nearby big cities…he emission-only simulation. Similarly, the NO_x emitted along major highways is transported to the surrounding grids, so that the atmospheric NO_x at the grids around the major highways become…ecomes isotop ... [18]

Formatted: Font color: Auto

Deleted: EGU located in the southwestern border of the state of Illinois,…outhern Illinois' Baldwin Energy Complex (marked with a transparent white box on Fig. 3b), us ... [19]

Formatted: Font: Symbol

Deleted: and in… In this time snapshot,…(06 UTC on Jul 26), the northeastwards propagating plume of NO_x emission from the EGU creates higher $\delta^{15}N(NO_x)$…$^{5}NO_x$ over ... [20]

Formatted: Font color: Black

Deleted: 23…‰ under the "no transport…mission only" scenario to -11.49…‰ under the "with ... [21]

Formatted: Font color: Auto

transport" scenario. While "emission only" $\delta^{15}N$ pattern shows biogenic emission dominating the spatial domain, in the "emission + transport" simulation anthropogenic emissions, becomes dominant over most of the grids, especially for the grids located around major cities' power plants.

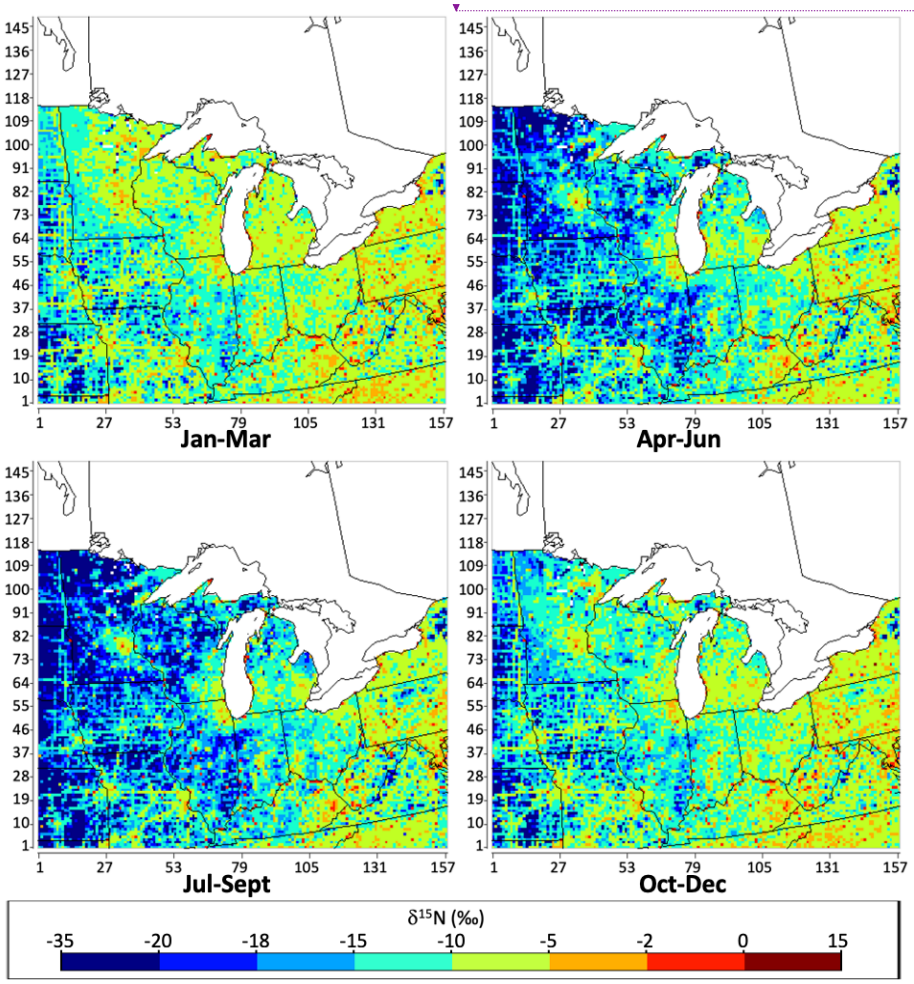

Figure 7: The geographical distribution of the $\delta^{15}N$ value of total NO_x emissions in each season (Winter: Jan-Mar; Spring: Apr-Jun; Summer: Jul-Sep; Fall: Oct-Dec) in per mil (‰) throughout the Midwest simulated by SMOKE, based on NEI-2002.

Deleted: The overall

Deleted: of the $\delta^{15}N$ value

Deleted: that the

Deleted: dominates

Formatted: Font color: Auto

Deleted: but after considering the atmospheric processes,

Deleted: emission, mainly from on-road vehicles

Formatted: Font color: Text 1

Deleted: in the suburb of

Deleted: cities

Formatted: Font color: Auto

Formatted: Font: 12 pt, Font color: Black

Formatted: Centered

Deleted:

3.3 Seasonal variation in $\delta^{15}NO_x$

We next examine the temporal heterogeneity of $\delta^{15}NO_x$ values over the domain for "emission only) and interpret them in terms of changes in NO_x emission fractions as a function of time. The predicted $\delta^{15}N$ value of total NO_x emissions in the Midwest during each season shows a significant temporal variation (Fig. 7). The $\delta^{15}NO_x$ ranged from -35 ‰ to 15 ‰, with the annual average over the Midwest at -6.15 ‰. The maps for different seasons show the obvious changes in $\delta^{15}N$ values over western regions of the Midwest, from green ($\delta^{15}N$ = -15 ~ -5 ‰) to dark blue (-35 ~ -15 ‰) during the month from April to October.

In order to qualitatively analyze the changes in $\delta^{15}NO_x$ among each season, the value of each grid (Fig. 7) were organized into the histograms (Fig. S6), in order to show the percentage of the grid in each color scheme. The grids with $\delta^{15}NO_x$ between -35‰ and -18‰ increase dramatically from less than 10% during fall (Oct-Dec) and winter (Jan-Mar) to more than 20% during spring (Apr-Jun) and summer (Jul-Sep). The grids with $\delta^{15}NO_x$ between -18‰ and -2‰ decrease from around 90% during fall and winter to around 75% during spring and summer. In addition, the distribution of $\delta^{15}NO_x$ shifts to lower values during spring and summer.

The significant temporal variation in the $\delta^{15}N$ value of total NO_x during different seasons can be quantitatively explained by changing fractions of NO_x emission from the biogenic source in any grid (Fig. S7) using Eq. (6). Unlike other NO_x emission sources, the fraction of NO_x emission from biogenic sources changes significantly among each season within the geographic domain, especially over the rural areas of the states of Minnesota, Iowa, Missouri, Wisconsin, Illinois, Indiana, Kentucky, Michigan, and Ohio (Fig. S7). The fraction of NO_x emission from biogenic sources over these areas increases from less than 0.25 to more than 0.50 during the months of April to October, which is the growing season. During this period, the surface sunlight hours, temperature, and precipitation are relatively higher and as a result, the canopy coverage of the plants becomes higher, which leads to the increase of the NO_x emission from biogenic sources (Pierce, 2001; Vukovich & Pierce, 2002; Schwede et al., 2005; Pouliot & Pierce, 2009; USEPA, 2018a). Besides this, the fertilizer application during this period is also responsible for the increase in soil NO_x emission (Li & Wang, 2008; Felix & Elliott, 2014).

In order to qualitatively analyze the changes in the fraction of NO_x emission from biogenic sources among each season, the distributions of the fractions among the same cut-offs as the maps on Fig. S7 were shown in the histograms (Fig. S8). Comparing the distributions of the fractions of NO_x emission from biogenic sources among the histograms for each season, the effects from the increasing of biogenic NO_x emission during the growing season of plants are clearly shown. In general, the distribution of the fraction shifts to higher values during spring (Apr-Jun) and summer (Jul-Sep), indicating the increase of biogenic emissions. As a result, the distribution of $\delta^{15}NO_x$ shifts to lower values during the same period (Fig. 7). The percentage of the grids with the fraction of biogenic emission less than 0.125 decreases dramatically from more than 50% during fall (Oct-Dec) and winter (Jan-Mar) to less than 35% during spring (Apr-Jun) and summer (Jul-Sep). As the NO_x emission from biogenic source becomes dominant, the percentage of the grids with $\delta^{15}NO_x$ between -35‰ and -18‰ increases, while the percentage of the grids with $\delta^{15}N(NO_x)$ between -18‰ and -2‰ decreases, which sufficiently explains the trends shown on Fig. 7.

Formatted: Font: Times New Roman, 12 pt

Deleted: ^{15}N of NO_x

Formatted: Add space between paragraphs of the same style, Outline numbered + Level: 2 + Numbering Style: 1, 2, 3, … + Start at: 1 + Alignment: Left + Aligned at: 0" + Indent at: 0.25"

Formatted: Font: 12 pt

Formatted: Font: Times New Roman, 12 pt

Deleted:

Moved (insertion) [11]

We then examine the temporal heterogeneity of atmospheric $\delta^{15}NO_x$ under the "emission + transport" scenario over the domain and interpret them in terms of changes in the propagation of NO_x emission as a function of time. The predicted seasonal average $\delta^{15}NO_x$ in the Midwest shows significant variations (Fig. 8). On an annual basis, the $\delta^{15}NO_x$ values range from -19.2‰ to 11.6‰, with the annual average over the Midwest domain of -6.10‰. Compared with the seasonal $\delta^{15}NO_x$ under the "no transport" scenario, the $\delta^{15}NO_x$ under the "with transport" scenario has a similar overall average while narrower range, due to the transport and mixing of the air mass. This could be clearly shown on the map, of which the color scheme is smoother, comparing with the seasonal $\delta^{15}N(NO_x)$ under the "no transport" scenario (Fig. 7). The maps for different seasons show the obvious changes in $\delta^{15}N$ values over western regions of the Midwest, from -8.75 ~ -5‰ in Oct-Mar to -16.25 ~ -12.5‰ in Apr-Oct.

In addition to the variability of the NO_x emission source, the significant temporal variation in the $\delta^{15}N$ value of atmospheric NO_x during different seasons is controlled by the transport and mixing of the air mass, under the different meteorology conditions that vary by season. The PBL height is an effective indicator showing whether the pollutants are under the synoptic condition, which is favorable for the dispersion, mixing, and transport after being emitted into the atmosphere (Oke, 2002; Shu et al., 2017; Liao et al., 2018; Miao et al., 2019). In order to qualitatively analyze the changes in $\delta^{15}N$ values driven by atmospheric processes, the difference between the $\delta^{15}N$ value of atmospheric NO_x under the "emission + transport" scenario and "emission only" scenario ($\Delta\delta^{15}N_{transport}$) on the seasonal basis were shown (Fig. S9). The seasonal $\Delta\delta^{15}N_{transport}$ values range from -21.9‰ to 31.2‰, with an average of 4.9‰. The overall pattern of the $\Delta\delta^{15}N_{transport}$ values shows that after the NO_x being emitted into the atmosphere, it became isotopically heavier over the majority of the grids within the domain, and isotopically lighter over the grids that contain big cities, major highways, and power plants. This could be explained by the transport and dispersion of biogenic emissions and anthropogenic emission to the surrounding areas. Among the grids located in rural areas, where the biogenic emission dominates the NO_x budget, the $\delta^{15}N$ values increases from around -30‰ to around -10‰, due to transport and dispersion of anthropogenic emission with relatively high emission rates from surrounding cities, highways, or power plants, which brings the isotopically heavier NO_x into the grids. On the other hand, among the grids located in the urban area, highways, or power plants, where anthropogenic emission dominates the NO_x budget, the changes in $\delta^{15}N$ values decrease is much less obvious, showing the $\Delta\delta^{15}N_{transport}$ values ranges between -5‰ and +5‰. This could be explained by the relatively high rates of anthropogenic emissions. Thus, the effects of the transport and dispersion of biogenic emissions from the surrounding rural area are minimal.

Deleted: $^{15}N(NO_x)$
Formatted: No grid
Deleted: with
Deleted: if
Deleted: $\delta^{15}N(NO_x)$
Deleted: 4
Deleted: $\delta^{15}N$
Deleted: of NO_x
Deleted: ‰, under the "with transport" scenario.
Deleted: $^{15}N(NO_x)$
Deleted: (Fang & Michalski, 2020),
Deleted: $^{15}N(NO_x)$
Deleted: driven by the atmospheric processes.
Deleted: S3
Deleted: which has been discussed in depth in the previous companion paper (Fang & Michalski, 2020),
Deleted: pollutant is
Deleted: disperse
Deleted: with
Deleted: no transport
Deleted: 5
Deleted: 95
Deleted: 22
Deleted: 93
Deleted: disperse
Deleted: emission
Deleted: disperse
Deleted: emission
Deleted: disperse

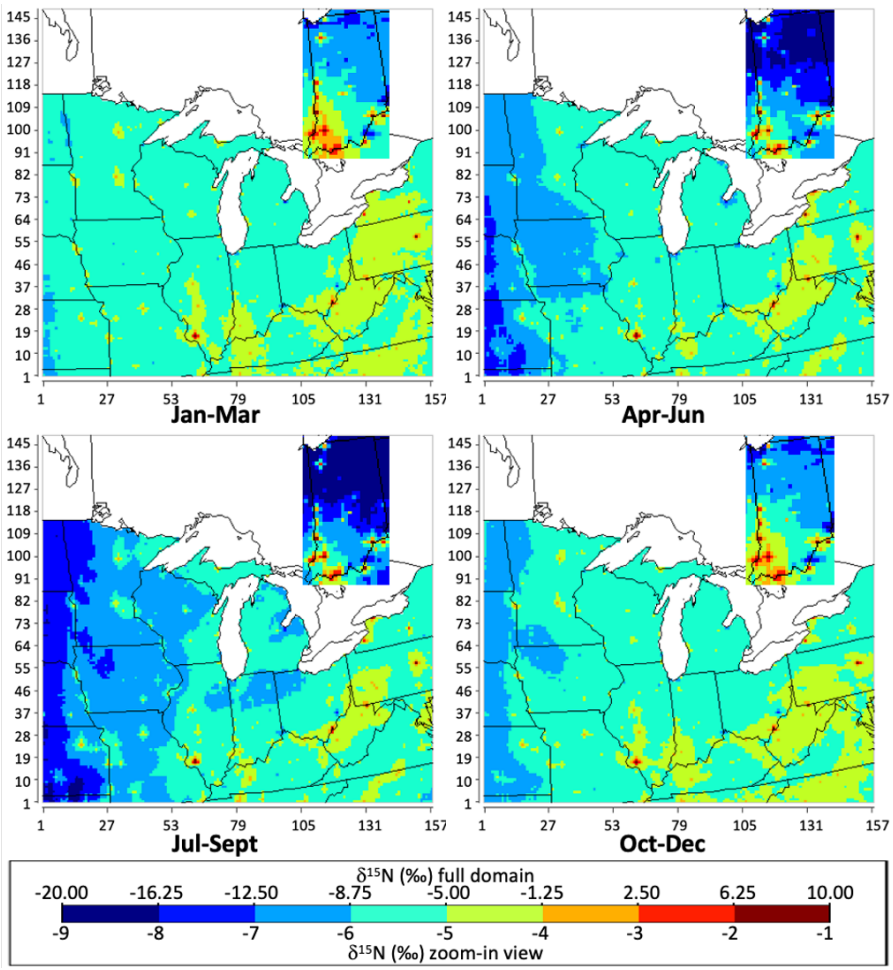

Figure 8: The geographical distribution of the $\delta^{15}N$ value of atmospheric NO_x in each season (Winter: Jan-Mar; Spring: Apr-Jun; Summer: Jul-Sep; Fall: Oct-Dec) in per mil (‰) throughout the Midwest (with zoom-in view focusing on Indiana) simulated by CMAQ, based on NEI-2002 and 2016 meteorology.

Comparing the distributions of the difference in $\delta^{15}N$ values (Fig. S9) with the corresponding PBL height (Fig. S10) among the maps of each season, the effects of PBL height on the propagation of the air mass are clearly shown. The PBL height changes significantly among each season within the geographic domain, especially over Minnesota, Wisconsin, and

Formatted: Left, First line: 0 ch

Deleted: 5

Deleted: S4

Iowa (Fig. S10). The PBL height over these areas increases from less than 250 meters above the ground level to more than 625 meters above the ground level, during spring (Apr-Jun) and summer (Jul-Sep), which creates a more favorable synoptic condition for the dispersion, mixing, and transport of the pollutants after being emitted into the atmosphere. As a result, the difference in $\delta^{15}N$ values shifts to higher values, showing the stronger effect of atmospheric processes during spring and summer. In order to qualitatively analyze how PBL height affects the level of the dispersion, mixing, and transport of the pollutants, the average $\delta^{15}N$ value of atmospheric NO_x along the plumes of power plants was compared with the domain average PBL height for each month within the Midwest region. The time series plot (Fig. 9a) shows the same seasonal trend of $\delta^{15}N$ values along the power plants plumes and PBL heights over the domain. Interestingly, the "turning point" of the $\delta^{15}N$ values is about one month later than the "turning point" of the PBL heights. The scatter plot (Fig. 9b) shows a strong positive correlation between the domain average PBL height and average $\delta^{15}N$ value along the power plants plumes, with R^2=0.85. The positive correlation between PBL height and propagation of air mass, indicated by the evolution of atmospheric $\delta^{15}NO_x$ in this study, agrees well with the corresponding measurement in megacities in China from the previous studies (Shu et al., 2017; Liu et al., 2018; Liao et al., 2018).

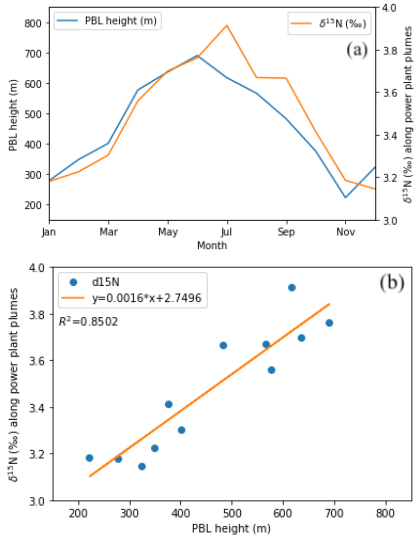

Figure 9: The time series plot (a) and the scatter plot (b) of the domain average PBL height (m) and the average $\delta^{15}N$ (‰) value of atmospheric NO_x along the plumes of power plants during each month throughout the Midwest simulated by CMAQ, based on NEI-2002 and 2016 meteorology.

Deleted: S4

Deleted: area

Deleted: disperse

Deleted: pollutant

Deleted: $^{15}N(NO_x)$

Deleted:

Formatted: Font color: Black

Deleted: *<object>*

*<object>*Different meteorology conditions

<object>

The atmospheric $\delta^{15}NO_x$ simulated based on different meteorology input dataset varies. In order to compare the spatial heterogeneity of the atmospheric $\delta^{15}NO_x$ under different meteorology conditions, the same analysis was done on the simulation using 2002 meteorology (Fig. S12). Overall, the simulated atmospheric NO_x under 2002 meteorology has the similar geographic distribution and seasonal trend as the 2016 simulation. In order to qualitatively compare the propagations of the pollutants under the impact of PBL height, the same plots were generated for simulation based on 2002 meteorology (Fig. 10). Comparing to the two simulations (Fig. 10a) reveals a similar seasonal trend but stronger monthly variation. Starting with lower PBL height during the winter, the corresponding $\delta^{15}N$ values along the power plants' plumes were lower, comparing to the simulation based on 2016 meteorology. As a result, the $\delta^{15}N$ values during the spring and summer were also relatively lower. On the other hand, due to the higher PBL height during the spring and summer for the simulation based on 2002 meteorology, the $\delta^{15}N$ values decreased slower since July, ending with the relatively higher $\delta^{15}N$ values in December. The scatter plot for the simulation based on 2002 meteorology (Fig. 10b) also shows a strong positive correlation between the domain average PBL height and average $\delta^{15}N$ value along the power plants plumes, with R^2=0.78. The videos of atmospheric $\delta^{15}NO_x$ on an hourly basis throughout the years 2002 and 2016 are available on Zenodo.org (10.5281/zenodo.4311986).

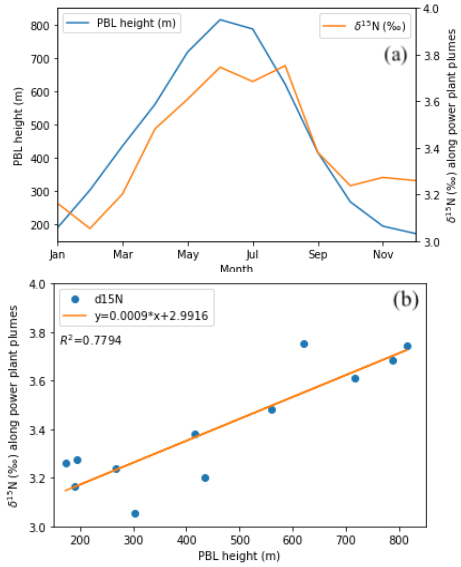

Figure 10: The time series plot (a) and the scatter plot (b) of the domain average PBL height (m) and the average $\delta^{15}N$ (‰) value of atmospheric NO_x along the plumes of power plants during each month throughout the Midwest simulated by CMAQ, based on NEI-2002 and 2002 meteorology.

3.4 The simulation over the extracted domain

Deleted: $^{15}N(NO_x)$

Deleted: $^{15}N(NO_x)$

Deleted: S6

Deleted: is isotopically heavier than

Formatted: Font color: Auto

Formatted: Font color: Auto

Deleted: , especially in the western part of the domain during summer (Fig. 6). The dynamics of PBL height potentially cause the variation in the level of disperse, mixing, and transport of NO_x emission. Due to the significantly higher level of PBL

Formatted: Font color: Auto

Formatted: Font color: Auto

Deleted: (Fig. 7) comparing

Formatted: Font color: Auto

Deleted: seasonal

Formatted: Font color: Auto

Deleted: 2016, the disperse, mixing, and transport of anthropogenic NO_x emission with higher $\delta^{15}N$ values alters the atmospheric $\delta^{15}N(NO_x)$ over the rural area further, under

Deleted: .

Formatted: Font color: Auto

Deleted: $^{15}N(NO_x)$

Deleted: year

Deleted: ¶
Different versions of emission inventories¶
There was a dramatic difference in the atmospheric $\delta^{15}N(NO_x)$ simulated depending on which NEI emission dataset was used. In order to compare the spatial heterogeneity of the atmospheric $\delta^{15}N(NO_x)$ generating from different NO_x emission budgets, the same analysis was done on the simulation using the emission input dataset prepared from the 2016 version of NEI (Fig. S7). In general, the simulated atmospheric NO_x based on 2016 NEI is significantly isotopically lighter than based on 2002 NEI, especially in the central and eastern parts of the domain (Fig. 8). According to Fang & Michalski (2020), the fraction of NO_x emission from the anthropogenic source in NEI-2016 was lower than in NEI-2002 for most of the grids within the domain. Therefore, the atmospheric $\delta^{15}N(NO_x)$ based on 2016 NEI was lower. According to US Energy Information Administration (2017b), from 2002 to 2016, 53 Giga Watts coal-fired and 54 Giga Watts natural gas EGU retired in the US. The EGU dominates the NO_x emission at the grids where it is located in, account for up to 90% of the total NO_x emission (Fang & Michalski, 2020). Given the $\delta^{15}N$ value of the NO_x emitted from coal-fired EGU is +15‰ (Table 1), the $\delta^{15}N$ values of the atmospheric NO_x over the grids that contain the abandoned coal-fired EGU change dramatically during the period between 2002 and 2016. A similar pattern occurs at the grids that contain the EGU, which uses both coal and natural gas as its energy source ($\delta^{15}N$ = -0.7 ... [22]

The temporal heterogeneity of difference in atmospheric $\delta^{15}NO_x$ between extracted-domain simulation and full-domain simulation ($\Delta\delta^{15}N_{extracted\text{-}full}$), to explore the potential bias due to the motion of the air mass across the boundary of the geographic domain of the study (Fig. 11). The extracted domain covers the states of Indiana, Illinois, Ohio, and Kentucky, where the measurements of $\delta^{15}NO_3^-$ at NADP sites are available. The predicted $\delta^{15}N$ of atmospheric NO_x over the extracted domain shows a similar overall pattern as the $\delta^{15}N$ within the same domain from the full-domain simulation, except over the southern border of the domain (Fig. S14). In order to qualitatively analyze the effects from the initial boundary condition, the $\delta^{15}N$ of atmospheric NO_x within IN, IL, OH, and KY were extracted from the full-domain simulation (Fig. 8) and compared with the extracted-domain simulation within the same region (Fig. 11). The $\Delta\delta^{15}N_{extracted\text{-}full}$ values ranged between -0.25‰ and +0.25‰ over most of the grids within the extracted domain, showing the difference between extracted-domain simulation and full-domain simulation of $\delta^{15}N$ values are trivial. However, near the southern border of the extracted domain, the obvious $\Delta\delta^{15}N_{extracted\text{-}full}$ values close to +0.75‰ during fall and winter, close to +1.00‰ during spring and summer occur, which indicate the atmospheric NO_x from the extracted-domain simulation is isotopically heavier. The values of $\Delta\delta^{15}N_{extracted\text{-}full}$ become obvious near the southern border, which indicates the dilution of NO_x, after it transports out of the domain since the $\delta^{15}N$ on the boundary was set to zero. Unlike the southern border, the northern, western, and eastern border of the extracted domain is located a sufficient distance apart from the boundary of the full domain. As a result, the $\Delta\delta^{15}N_{extracted\text{-}full}$ values are similar over the majority grids within the domain.

Moved up [9]: ¶
We next examine the

Formatted: Indent: First line: 0 ch

Formatted: Font: 12 pt

Moved up [11]: S8).

Moved down [12]: The complete isotope effect of tropospheric photochemistry will be addressed in future work, which incorporates ^{15}N into the chemical mechanism of CMAQ for the simulation.

Deleted: role of deposition¶
The deposition alters the $\delta^{15}N$ of atmospheric NO_x. In order to compare the spatial heterogeneity of the atmospheric $\delta^{15}N(NO_x)$ with different settings of NO_x deposition rate, the same analysis was done on the simulation using the amplified dry and wet deposition rates (Fig.

Deleted: In order to explore the impact of dry an ... [23]

Deleted: ¶ ... [24]

Formatted: Font: 12 pt

Deleted: $^{15}N(NO_x)$

Deleted: nested

Deleted: $^{15}N_{nested}$

Deleted: 10

Deleted: nested

Deleted: $\delta^{15}N$ values

Deleted: nested

Deleted:

Formatted ... [25]

Deleted: S9

Deleted: 4

Deleted: compare

Deleted: nested

Deleted: 10

Deleted: $^{15}N_{nested}$

Deleted: nested

Deleted: nested

Deleted: nested

Deleted: $^{15}N_{nested}$

Deleted: closed

Deleted: nested

Deleted: $^{15}N_{nested}$

Deleted: nested

Deleted: $^{15}N_{nested}$

Deleted:

Deleted:

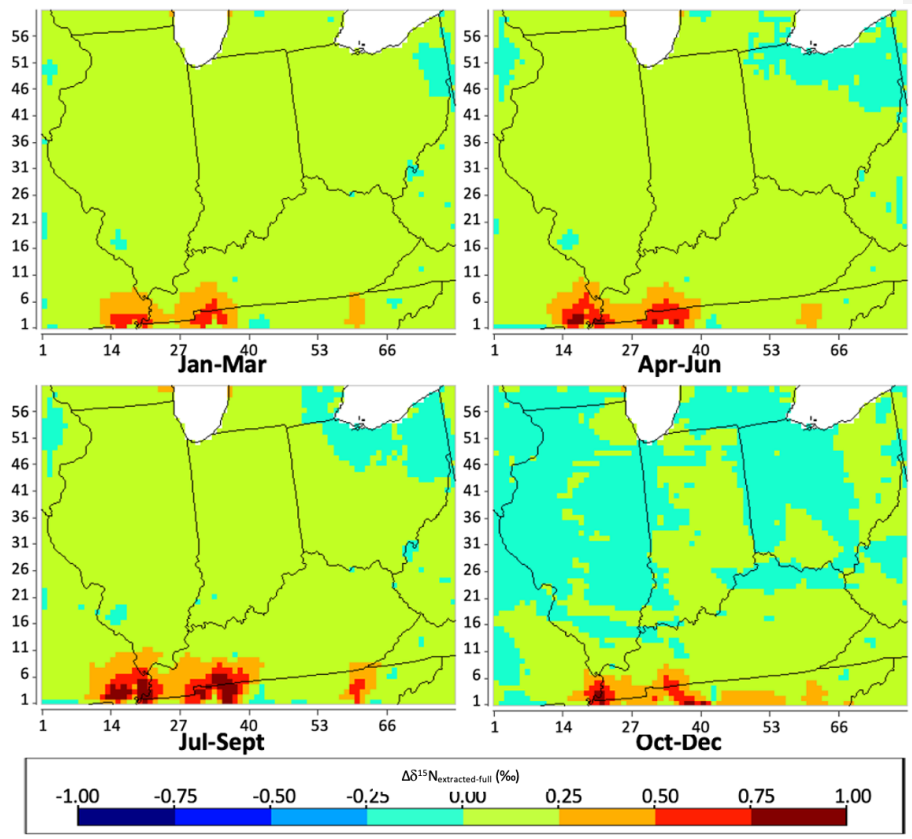

Figure 11: The geographical distribution of the difference between extracted-domain simulation and full-domain simulation of $\delta^{15}N$ value of atmospheric NO_x ($\Delta\delta^{15}N_{extracted\text{-}full}$) in each season (Winter: Jan-Mar; Spring: Apr-Jun; Summer: Jul-Sep; Fall: Oct-Dec) in per mil (‰) within IN, IL, OH, and KY, based on NEI-2002 and 2016 meteorology.

3.5 The role of enhanced NO_x deposition

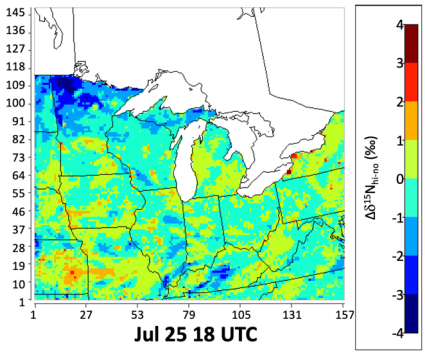

Figure 12. The $\Delta\delta^{15}N_{hi\text{-}no}$ values at 18 UTC on July 25.

The "emission + mixing + enhanced deposition" simulations significantly alter the $\delta^{15}N$ of atmospheric NO_x relative to the normal deposition scenarios. Again, the enhanced deposition cases are removing NO_x at rates that would be similar to those by removal during its conversion into HNO_3. Thus, in these cases the NO_x deposited is ~ $\delta^{15}NO_3^-$ and the $\delta^{15}NO_x$ is that in the residual NO_x. The impact of high deposition on the residual NO_x was assessed using $\Delta\delta^{15}N_{hi\text{-}no}$, the difference between the $\delta^{15}NO_x$ values of atmospheric under the "enhanced deposition" and "no deposition" scenarios. The $\Delta\delta^{15}N_{hi\text{-}no}$ range was ± 4‰ and was especially obvious downwind of the locations with large emission rates, such as power plants or megacities (Fig. 12a). This can be explained as a similar fashion to the "no deposition" scenarios (Fig. S15a), where the dispersion of the isotopically heavier NO_x emission from big cities, major highways, and power plants elevates the $\delta^{15}NO_x$ values in the surrounding grids located in rural areas, the dispersion of the isotopically lighter biogenic NO_x emission lowers the $\delta^{15}NO_x$ values in the surrounding grids located in the suburb of major cities (Fig. S15b). On the other hand, due to the higher deposition rate, the transport, mixing, and dispersion of NO_x emission from different sources are restricted within a smaller geographical extent (Fig. S15b). As a result, under the "enhanced deposition" scenario, the NO_x emissions disperse to fewer surrounding grids but lead to a lower $\delta^{15}NO_x$ values relative to no deposition. The temporal heterogeneity of $\Delta\delta^{15}N_{hi\text{-}no}$ over the domain was examined and the impact of enhancing deposition rates of NO_x on the $\delta^{15}N$ of atmospheric NO_x on the seasonal basis was explored (Fig. 14). The seasonal $\Delta\delta^{15}N_{hi\text{-}no}$ values range from -3.67‰ to 5.34‰, with an average of 0.51‰. The overall pattern of the $\Delta\delta^{15}N_{hi\text{-}no}$ values shows that due to deposition, the atmospheric NO_x became isotopically lighter over the majority of the grids since EGU and vehicle NO_x is not being transported as far in the enhanced deposition. Conversely, in grids that contain or surround power plants and big cities the $\delta^{15}NO_x$ increases because it is not as effectively mixing with low $\delta^{15}NO_x$ from nearby grids. The enhanced deposition simulation somehow presents the isotope effects associated with the "pseudo photochemical transformation" of NO_x into NO_y.

The complete isotope effect of tropospheric photochemistry will be addressed in future work, which incorporates ^{15}N into the chemical mechanism of CMAQ for the simulation.

Moved down [13]: ¶
Model-observation comparison

Moved (insertion) [12]

Moved down [14]: The $\delta^{15}N$ of the corresponding measurement ranges from -33.8‰ to 0.2‰, with the medium of -11.2 ± 8.0‰.

Deleted: In general, the CMAQ simulations of $\delta^{15}N(NO_x)$ under most of the scenarios conducted in this study, except the simulation based on NEI-2016 and 2016 meteorology, perform better than the SMOKE simulation of $\delta^{15}N(NO_x)$, which only take the variability of NO_x emission source into account (Table 2). On the other hand, the simulation based on NEI-2016 and 2016 meteorology capture the isotopically light NO_x better than the simulations under the other scenarios of emission and meteorology input datasets. ¶

Finally, we compared the CMAQ predicted $\delta^{15}N(NO_x)$, under the scenario of NEI-2002+WRF2002 at NADP sites within Indiana, Illinois, Ohio, and Kentucky (Table S3) with the measurements of $\delta^{15}N(NO_3^-)$ from 2001 to 2003. The $\delta^{15}N$ values of atmospheric NO_x

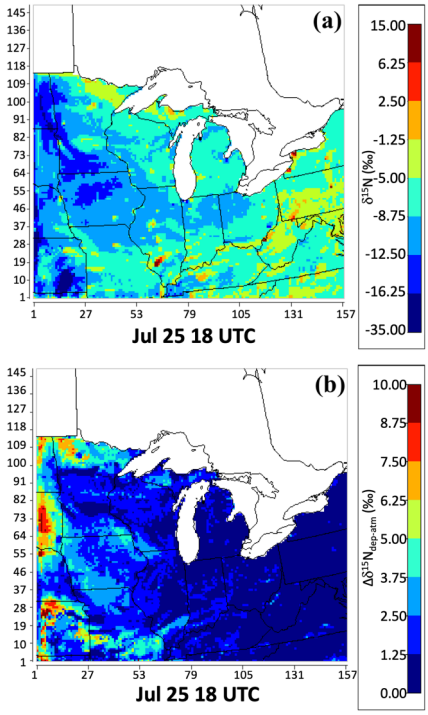

Figure 13: The $\delta^{15}N$ values of NO_x deposition under the "enhanced deposition" scenario (a); the $\Delta\delta^{15}N_{dep\text{-}atm}$ (b), at 18 UTC on July 25, are presented by color in each grid (NEI-2002 and 2016 meteorology). The warmer the color, the higher $\delta^{15}N$ and $\Delta\delta^{15}N_{deposition}$ values of atmospheric NO_x

The $\delta^{15}NO_x$ deposition (proxy for $\delta^{15}NO_3^-$) simulated by CMAQ at these sites show similar monthly variations and seasonal trends as SMOKE (Fig. S19). The ranges of $\delta^{15}N(NO_x)$ values within each month were narrower, comparing to the simulation from SMOKE, with a minimum during February (-8.7~ -4.4‰) and a maximum during August (-11.8~-4.2‰). The seasonal trend shows low $\delta^{15}N(NO_x)$ during summer, with the median around -7.4‰, and high $\delta^{15}N(NO_x)$ during winter, with the median around -6.0‰. Therefore, the CMAQ simulation inherits the monthly variations and seasonal trends from SMOKE, while the atmospheric NO_x becomes isotopically heavier, after taking atmospheric mixing and transport into account. As mentioned above, most of the NADP sites are located away from big cities and power plants. Thus, the atmospheric mixing and transport led to the isotopically heavier atmospheric NO_x.

Deleted: obvious

Deleted: 14, top). The monthly boxes are the 1st and 3rd quantiles of the simulated monthly $\delta^{15}N$ of atmospheric NO_x at the NADP sites. The whiskers represent the minimum and maximum values without outliers. There is a wide range

Deleted: January (-

Deleted: .8

Deleted: 1

Deleted: 4

Deleted: 4

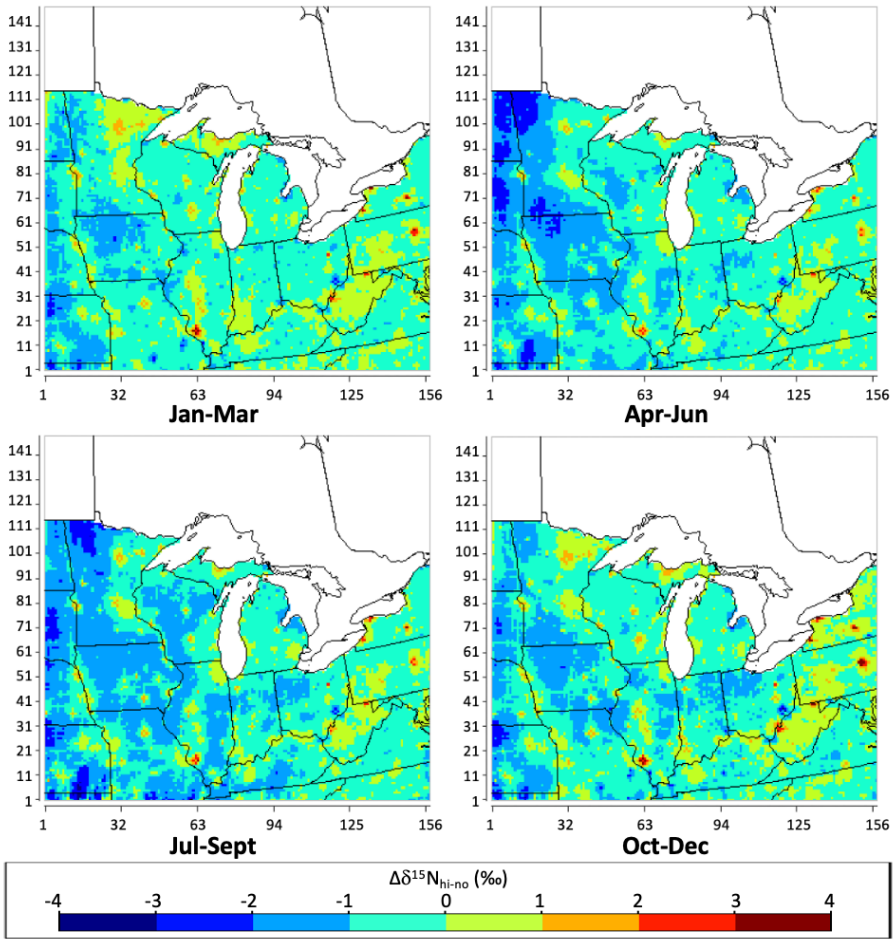

Figure 14: The difference between the $\delta^{15}N$ (‰) value of atmospheric NO_x under the "enhanced deposition" scenario and "no deposition" scenario ($\Delta\delta^{15}N_{hi\text{-}no}$) during each season (Winter: Jan-Mar; Spring: Apr-Jun; Summer: Jul-Sep; Fall: Oct-Dec), throughout the Midwest simulated by CMAQ, based on NEI-2002 and 2016 meteorology.

3.6 Model-observation comparison of $\delta^{15}NO_x$

Moved (insertion) [13]

Formatted: Indent: First line: 0.25"

Deleted: Comparing with

Formatted: Font: Times New Roman, 12 pt

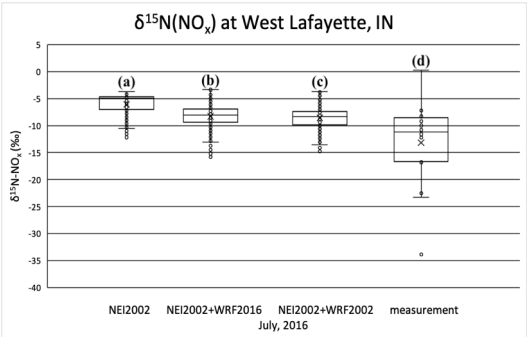

Figure 15: The $\delta^{15}NO_x$ distributions for Lafayette, IN from July 8 to August 5, simulated by SMOKE (a), CMAQ based on 2016 (b) and 2002 meteorology (c), compare with the measured $\delta^{15}NO_x$ (d) taken on July to August in 2016 (box: lower quartile, median, upper quartile; whisker: lower extreme, upper extreme; dots outside the whisker: outliers)

In order to evaluate the SMOKE/CMAQ simulations of atmospheric $\delta^{15}N$, they were compared to several existing observational datasets. The $\delta^{15}N$ values under the "no transport" simulation by SMOKE in West Lafayette, IN was compared with the measurement (Walters, Fang, & Michalski, 2018) from July 8 to August 5, 2016 (Fig. 15). The range of SMOKE simulated $\delta^{15}N(NO_x)$ from NEI-2002 ranges from -12.2‰ to -3.8‰, which is within the range of the corresponding measurement (-33.8 ~ 0.2 ‰). Whereas the median (-5.0 ± 2.2 ‰) of SMOKE simulated $\delta^{15}N(NO_x)$ is higher than the median (-11.2 ± 8.0 ‰) of the measured values. The SMOKE simulated $\delta^{15}N(NO_x)$ values in West Lafayette, IN are higher than the corresponding measurements. Therefore, the emission from the soil, livestock waste, off-road vehicles, and natural gas power plant might be underestimated, and/or the emission from the on-road vehicle and coal-fired power plant might be overestimated for both versions of NEI.

In addition to the effects from NO_x emission sources, the lower values and greater variations in measured $\delta^{15}N(NO_x)$ might also be caused by the atmospheric mixing with the emission from surrounding grids, driven by the atmospheric processes. The $\delta^{15}N$ of atmospheric NO_x under the "with transport" scenario by CMAQ with different meteorology conditions (simulated by WRF for the year 2002 and 2016) was compared with the measurement (Walters, Fang, & Michalski, 2018) from July 8 to August 5, 2016 (Fig. 15). The $\delta^{15}N$ of atmospheric NO_x simulated based on 2016 meteorology ranges from -15.8‰ to -3.4‰, with the medium of -8.1 ± 2.1‰; the $\delta^{15}N$ of atmospheric NO_x simulated based 2002 meteorology ranges from -14.8‰ to -3.7‰, with the medium of -8.4 ± 1.9‰. The $\delta^{15}N$ of the corresponding measurement ranges from -33.8‰ to 0.2‰, with the medium of -11.2 ± 8.0‰. In general, the CMAQ simulations of $\delta^{15}N(NO_x)$ under both of the scenarios conducted in this study perform better than the SMOKE simulation of $\delta^{15}N(NO_x)$, which only takes the variability of the NO_x emission source into account (Table S7).

Moved (insertion) [14]

Deleted: , the

3.7 Enhanced NO_x deposition simulating $\delta^{15}NO_3$: model observation comparison

The model was used to predict $\delta^{15}NO_3^-$ and compared with the $\delta^{15}NO_3^-$ in deposition collect between 2001 and 2003 at several Midwestern NADP sites (Table S4). The measurements of $\delta^{15}N$ values of NO_3^- at NADP sites from prior studies (Mase, 2010; Riha, 2013) show the similar monthly variations and seasonal trend as both "no transport" and "with transport" simulations (Fig. S19). There is a wide range of $\delta^{15}N(NO_3^-)$ values within each month, with a minimum during January (10.4~17.2‰) and a maximum during August (1.0~16.7‰). The seasonal trend shows low $\delta^{15}N(NO_3^-)$ during spring, with the median around 9.3‰, and high $\delta^{15}N(NO_3^-)$ during winter, with the median around 13.0‰. The measured $\delta^{15}N$ values of NO_3^- have the same seasonal trend as the simulated $\delta^{15}N$ values of NO_x. Even considering the effect of atmospheric mixing and transport, the measured $\delta^{15}N$ values of NO_3^- is about 17‰ higher than the simulated $\delta^{15}N$ values of NO_x. The difference between CMAQ simulated and measured $\delta^{15}N$ values of deposition is caused by the following two factors: a). the mixture of isotopically lighter NO_x from the surrounding area discussed in section 3.3, and b). the net N isotope effect during the conversion of NO_x to NO_3^-, which will be addressed in future work.

Formatted: Indent: First line: 2 ch

Deleted: shows

Deleted: (Fig. 14, bottom

Deleted: has

Deleted: CMAQ

Deleted: However

Deleted: CMAQ

Deleted: $\delta^{15}N$ values of NO_x

Deleted: NO_3^-

Deleted: 2

Deleted:

Formatted: Font: 12 pt

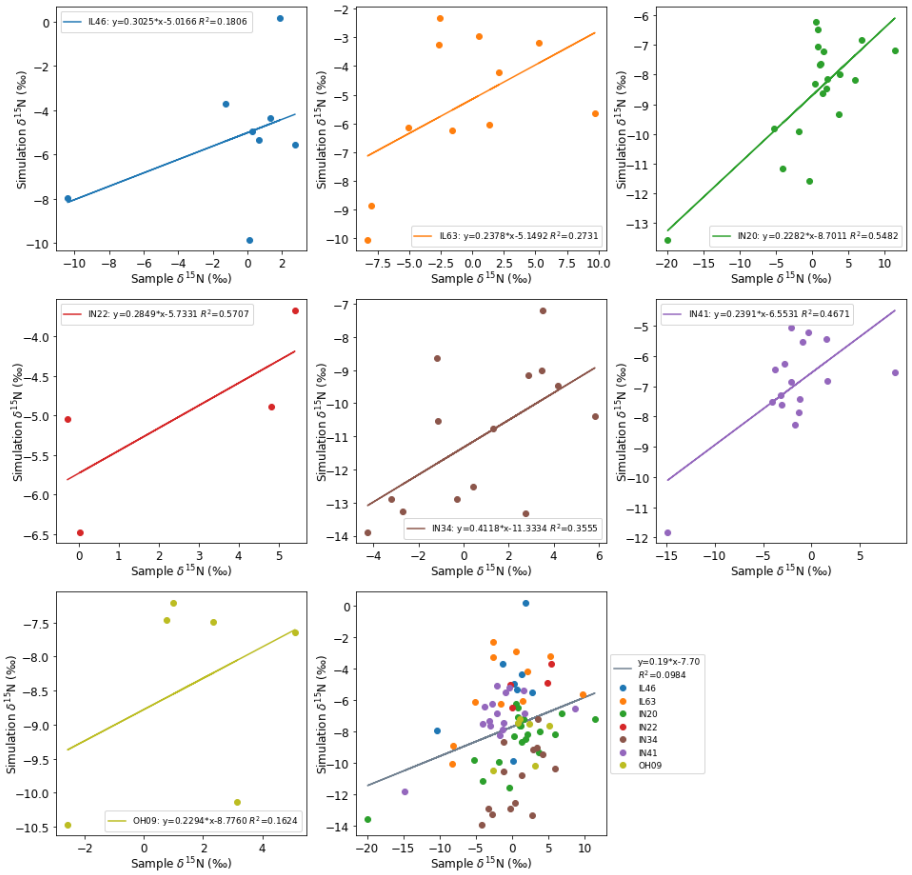

Figure 16: The emission + mixing + deposition CMAQ predicted $\delta^{15}N$ value of NO_x deposition using NEI-2002 and 2002 meteorology compared to the measured $\delta^{15}N$ of rain NO_3^- at NADP sites within IN, IL, and OH.

The 30 fold enhanced NO_x deposition (see methods) was used to simulate the $\delta^{15}N$ value of NO_3^- deposition ($\delta^{15}N(NO_3^-)$) that was then compared to observations (Fig. 16). As previously noted, rather than explicitly converting NO_x into NO_y via the chemical mechanism in CMAQ, which would require writing an isotope-enabled chemical scheme with appropriate rate constants, we amplified NO_x deposition as a surrogate. This amplification reduced the NO_x lifetime to about 1 day, thus by calculating the $\delta^{15}N$ of NO_x in the deposition fraction, as opposed to residual NO_x in the atmosphere, we are approximating the $\delta^{15}N(NO_3^-)$ in deposition. The model approximation was compared to NO_3^- collected at NADP sites within Indiana, Illinois, and Ohio in the year 2002 (Table S4). The NEI-2002 and WRF2002 were used for the SMOKE emission model and CMAQ simulations, respectively. The $\delta^{15}N(NO_3^-)$ value in deposition was calculated by $\delta^{15}N(NO_3^-) = \Sigma$

f_{NOxhr} $\delta^{15}N(NO_x)_{hr}$, where f_{NOxhr} is the hourly mole fraction of NO_x isotopologue deposited (f_{NOxhr} = NO_{xhr}/NO_{xT}) and $\delta^{15}N(NO_x)_{hr}$ is the $\delta^{15}N$ value of NO_x in deposition. The total NO_x deposited (NO_{xT}) used to calculate f_{NOxhr} was the amount deposited 5 days prior to the sampling date since the NADP deposition collection integrate the week. The $\delta^{15}N$ values of NO_x deposition simulated by CMAQ under the "enhanced deposition" scenario at each site were compared with the measurements of $\delta^{15}N$ values of NO_3 from prior studies (Mase, 2010; Riha, 2013). The scatter plots show moderate positive correlation between sample $\delta^{15}N$ and simulated $\delta^{15}N$, with R^2 between 0.16 and 0.57 (Fig. 16). The difference in the trend line equations among the NADP sites might be caused by the difference in air temperature and photolysis rate, which impact the chemical mechanisms converting NO_x into NO_y and will be explored in future study.

4. Conclusion

The $\delta^{15}N$ of atmospheric NO_x was simulated by SMOKE, by considering the NO_x emissions from NEI emission sectors and the corresponding $\delta^{15}N$ values from previous research. $\delta^{15}N$ is an effective tool to track the atmospheric NO_x, in terms of its evolution of spatial and temporal composition, altered by atmospheric processes The simulation indicates that the NO_x emission from biogenic sources is the key driver for the variation of $\delta^{15}N$, especially among the NADP sites. The uncertainties in the $\delta^{15}N(NO_x)$ simulation are less than 5‰ over the majority of the grids within the Midwest. For the NO_x emission from the regions dominated by biogenic source, the uncertainties in the $\delta^{15}N(NO_x)$ simulation are less than 10‰. The uncertainties in the $\delta^{15}N(NO_x)$ simulation were well below the difference among the $\delta^{15}N(NO_x)$ values from different NO_x emission sources (Fig. S20). Comparing with the measurements of $\delta^{15}N(NO_3^-)$ from NADP sites within Indiana, Illinois, Ohio, and Kentucky, the simulated $\delta^{15}N$ agreed well with the seasonal trend and monthly variation. While the simulated NO_x is slightly heavier than the corresponding measurements in West Lafayette, IN, taken from July to August 2016. According to the previous research, the uncertainty of NO_x emission is 71-250% from soil and 10-15% from the vehicle. The variations among the removal efficiency of different emission control technologies vary from 30% to 90%, also causes the uncertainty of power plant NO_x emission. In addition, in this study, due to the lack of measurements, the $\delta^{15}N$ of coal-fired and natural gas non-EGUs (industrial boilers, commercial and residential fuel combustions) were assumed to be the same as the $\delta^{15}N$ of coal-fired and natural gas EGUs respectively. Thus, detailed measurements of the $\delta^{15}N$ of non-EGUs are necessary for future study. Besides this, the non-road vehicles (aircraft, ships, and trains) also need to be included in the future study.

If we only consider the effects from NO_x emission sources, the emission from soil, livestock waste, off-road vehicles, and natural gas power plant in West Lafayette, IN are possible to be underestimated, and the emission from the on-road vehicle and coal-fired power plant in West Lafayette, IN are possible to be overestimated. Another reason causing the estimated NO_x isotopically heavier than measured NO_x is the mixing caused by atmospheric processes, since the NO_x emission from the surrounding region of West Lafayette, IN is lighter. In addition, the tropospheric photochemistry could also alter the $\delta^{15}N$ values during the processes that convert NO_x to NO_y.

After considering the impacts of atmospheric processes, by simulating CMAQ based on the ^{15}N incorporated emission input datasets and the meteorology input dataset simulated from WRF and MCIP, the performance of the simulated $\delta^{15}N(NO_x)$ is better. The simulation indicates that the PBL height is the key driver for the mixture of anthropogenic and natural NO_x emission, which deepens the gap between $\delta^{15}N$ of atmospheric NO_x and NO_x emission. After considering the effects

Formatted: Font: 12 pt

Formatted: Font: Times New Roman, 12 pt

Formatted: Outline numbered + Level: 1 + Numbering Style: 1, 2, 3, … + Start at: 3 + Alignment: Left + Aligned at: 0" + Indent at: 0.25"

Moved (insertion) [15]

Deleted: The $\delta^{15}N$ of atmospheric NO_x was simulated by CMAQ, based on the emission input datasets prepared from the previous companion research (Fang & Michalski, 2020) and the meteorology input dataset simulated from WRF and MCIP. $\delta^{15}N$ is an effective tool to track the atmospheric NO_x, in term of its evolution of spatial and temporal composition, altered by atmospheric processes.

Moved up [15]: Comparing with the measurements of $\delta^{15}N(NO_3^-)$ from NADP sites within Indiana, Illinois, Ohio, and Kentucky, the simulated $\delta^{15}N$ agreed well with the seasonal trend and monthly variation.

Deleted: The performance of CMAQ simulated $\delta^{15}N(NO_x)$ is better than SMOKE $\delta^{15}N(NO_x)$ from the previous companion research (Fang & Michalski, 2020), due to the consideration of mixing, disperse, and transport of NO_x emission from different sources.¶

of NO_x emission sources and atmospheric processes, there is still an obvious gap between the simulated $\delta^{15}N(NO_x)$ and the corresponding measurements. Therefore, before adjusting the NO_x emission inventory, the future work is to explore how tropospheric photochemistry alters $\delta^{15}N(NO_x)$ by incorporating ^{15}N into the chemical mechanism of CMAQ and comparing the simulation with the corresponding measurements. With the validation of our nitrogen isotopes incorporated CMAQ, the NO_x emission inventories could be effectively evaluated and improved.

Data availability: The source code for SMOKE version 4.6 is available at https://github.com/CEMPD/SMOKE/releases/tag/SMOKEv46_Sep2018. The source code for CMAQ version 5.2.1 is available at https://github.com/USEPA/CMAQ/tree/5.2.1. The in-detail simulation results for $\delta^{15}N$ of NO_x emission based on 2002 and 2016 versions of National Emission Inventory and the associated python codes are achieved on Zenodo.org (10.5281/zenodo.4048992). The input datasets for WRF simulation are available at https://www.ncei.noaa.gov/data/. The in-detail simulation results for $\delta^{15}N$ of atmospheric NO_x under all scenarios discussed in this paper and the CMAQ-based c-shell script for generating BCON for extracted domain simulation are achieved on Zenodo.org (10.5281/zenodo.4311986).

Author contributions: Huan Fang and Greg Michalski were the investigator for the project and organized the tasks. Huan Fang develop the model codes, performed the simulation to incorporate ^{15}N into SMOKE outputs and generated $\delta^{15}N$ values and reconstruct CMAQ by incorporating ^{15}N, and performed the simulation to generate $\delta^{15}N$ values. Greg Michalski helped Huan Fang in interpreting the results. Huan Fang prepared the manuscript with contributions from all co-authors.

Acknowledgments: We would like to thank the Purdue Research Foundation and the Purdue Climate Change Research Center for providing funding for the project. We would like to thank Scott Spak from School of Urban & Regional Planning, University of Iowa for simulating SMOKE using NEI-2002. We would like to thank Tomas Ratkus from Department of Earth, Atmospheric, and Planetary Sciences, Steven Plite, and Frank Bakhit from Rosen Center for Advanced Computing, Purdue University for setting up CMAQ on Purdue research computing for this project.

Formatted: Font color: Black

Formatted: Font color: Black

Deleted: in-detail simulation results for $\delta^{15}N$ of atmospheric NO_x under all scenarios discussed in this paper and the CMAQ-based c-shell script for generating BCON for nested domain simulation are achieved on Zenodo.org (10.5281/zenodo.4311986).

Deleted: develops

Deleted: reconstruct CMAQ by incorporating ^{15}N and

References:

Almaraz, M., Bai, E., Wang, C., Trousdell, J., Conley, S., Faloona, I. and Houlton, B. Z.: Agriculture is a major source of NOx pollution in California, Sci. Adv., doi:10.1126/sciadv.aao3477, 2018.

Ammann, M., Siegwolf, R., Pichlmayer, F., Suter, M., Saurer, M. and Brunold, C.: Estimating the uptake of traffic-derived NO2 from 15N abundance in Norway spruce needles, Oecologia, doi:10.1007/s004420050710, 1999.

Beirle, S., Spichtinger, N., Stohl, A., Cummins, K. L., Turner, T., Boccippio, D., Cooper, O. R., Wenig, M., Grzegorski, M., Platt, U. and Wagner, T.: Estimating the NOx produced by lightning from GOME and NLDN data: A case study in the Gulf of Mexico, Atmos. Chem. Phys., doi:10.5194/acp-6-1075-2006, 2006.

Boersma, K. F., Eskes, H. J., Meijer, E. W. and Kelder, H. M.: Estimates of lightning NOx; production from GOME satellite observations, Atmos. Chem. Phys., doi:10.5194/acp-5-2311-2005, 2005.

Bradshaw, J., Davis, D., Grodzinsky, G., Smyth, S., Newell, R., Sandholm, S. and Liu, S.: Observed distributions of nitrogen oxides in the remote free troposphere from the NASA Global Tropospheric Experiment programs, Rev. Geophys., doi:10.1029/1999RG900015, 2000.

Byun, D., Pleim, J., Tang, R. and Bourgeois, A.: Meteorology-Chemistry Interface Processor (MCIP) for Models-3 Community Multiscale Air Quality (CMAQ) Modeling System, System, 1999.

Chameides, W. L., Davis, D. D., Bradshaw, J., Rodgers, M., Sandholm, S. and Bai, D. B.: An estimate of the NO x production rate in electrified clouds based on NO observations from the GTE/CITE 1 fall 1983 field operation , J. Geophys. Res., doi:10.1029/jd092id02p02153, 1987.

Chang, Y., Zhang, Y., Tian, C., Zhang, S., Ma, X., Cao, F., Liu, X., Zhang, W., Kuhn, T. and Lehmann, M. F.: Nitrogen isotope fractionation during gas-to-particle conversion of NOx to NO3- in the atmosphere - Implications for isotope-based NO x source apportionment, Atmos. Chem. Phys., doi:10.5194/acp-18-11647-2018, 2018.

Christian, H. J., Blakeslee, R. J., Boccippio, D. J., Boeck, W. L., Buechler, D. E., Driscoll, K. T., Goodman, S. J., Hall, J. M., Koshak, W. J., Mach, D. M. and Stewart, M. F.: Global frequency and distribution of lightning as observed from space by the Optical Transient Detector, J. Geophys. Res. Atmos., doi:10.1029/2002jd002347, 2003.

Cicero-Fernândez, P., Long, J. R. and Winer, A. M.: Effects of Grades and Other Loads on On-Road Emissions of Hydrocarbons and Carbon Monoxide, J. Air Waste Manag. Assoc., doi:10.1080/10473289.1997.10464455, 1997.

Dameris, M., Grewe, V., Ponater, M., Deckert, R., Eyring, V., Mager, F., Matthes, S., Schnadt, C., Stenke, A., Steil, B., Brühl, C. and Giorgetta, M. A.: Long-term changes and variability in a

Deleted:

Formatted: Justified

Formatted: Justified

Formatted: Justified

Formatted: Justified

transient simulation with a chemistry-climate model employing realistic forcing, Atmos. Chem. Phys., doi:10.5194/acp-5-2121-2005, 2005.

Davidson, E. A.: Pulses of nitric oxide and nitrous oxide flux following wetting of dry soil: an assessment of probable sources and importance relative to annual fluxes, Trace gas Exch. a Glob. Perspect., 1992.

Davidson, E. A. and Kingerlee, W.: A global inventory of nitric oxide emissions from soils, Nutr. Cycl. Agroecosystems, doi:10.1023/a:1009738715891, 1997.

de Foy, B., Lu, Z., Streets, D. G., Lamsal, L. N. and Duncan, B. N.: Estimates of power plant NOx emissions and lifetimes from OMI NO2 satellite retrievals, Atmos. Environ., doi:10.1016/j.atmosenv.2015.05.056, 2015.

De Laeter, J. R., Böhlke, J. K., De Bièvre, P., Hidaka, H., Peiser, H. S., Rosman, K. J. R. and Taylor, P. D. P.: Atomic weights of the elements: Review 2000 (IUPAC Technical Report), Pure Appl. Chem., doi:10.1351/pac200375060683, 2003.

DeCaria, A. J., Pickering, K. E., Stenchikov, G. L. and Ott, L. E.: Lightning-generated NOx and its impact on tropospheric ozone production: A three-dimensional modeling study of a Stratosphere-Troposphere Experiment: Radiation, Aerosols and Ozone (STERAO-A) thunderstorm, J. Geophys. Res. D Atmos., doi:10.1029/2004JD005556, 2005.

Dentener, F. J. and Crutzen, P. J.: Reaction of N2O5 on tropospheric aerosols: impact on the global distributions of NOx, O3, and OH, J. Geophys. Res., doi:10.1029/92JD02979, 1993.

Dignon, J. and Hameed, S.: Global emissions of nitrogen and sulfur oxides from 1860 to 1980, J. Air Waste Manag. Assoc., doi:10.1080/08940630.1989.10466519, 1989.

Dreher, D. B. and Harley, R. A.: A fuel-based inventory for heavy-duty diesel truck emissions, J. Air Waste Manag. Assoc., doi:10.1080/10473289.1998.10463686, 1998.

Duncan, B. N., Yoshida, Y., De Foy, B., Lamsal, L. N., Streets, D. G., Lu, Z., Pickering, K. E. and Krotkov, N. A.: The observed response of Ozone Monitoring Instrument (OMI) NO2 columns to NOx emission controls on power plants in the United States: 2005-2011, Atmos. Environ., doi:10.1016/j.atmosenv.2013.08.068, 2013.

Elliott, E. M., Kendall, C., Boyer, E. W., Burns, D. A., Lear, G. G., Golden, H. E., Harlin, K., Bytnerowicz, A., Butler, T. J. and Glatz, R.: Dual nitrate isotopes in dry deposition: Utility for partitioning NO x source contributions to landscape nitrogen deposition, J. Geophys. Res. Biogeosciences, doi:10.1029/2008JG000889, 2009.

Elliott, E. M., Kendall, C., Wankel, S. D., Burns, D. A., Boyer, E. W., Harlin, K., Bain, D. J. and Butler, T. J.: Nitrogen isotopes as indicators of NOx source contributions to atmospheric nitrate deposition across the midwestern and northeastern United States, Environ. Sci. Technol., doi:10.1021/es070898t, 2007.

Formatted: Justified

Formatted: Justified

Formatted: Justified

Moved (insertion) [16]

Formatted: Justified

Farrell, A., Carter, R. and Raufer, R.: The NOx Budget: Market-based control of tropospheric ozone in the northeastern United States, Resour. Energy Econ., doi:10.1016/S0928-7655(98)00035-9, 1999.

Fehr, T., Höller, H. and Huntreiser, H.: Model study on production and transport of lightning-produced NOx in a EULINOX supercell storm, J. Geophys. Res. D Atmos., doi:10.1029/2003JD003935, 2004.

Felix, J. D., Elliott, E. M. and Shaw, S. L.: Nitrogen isotopic composition of coal-fired power plant NOx: Influence of emission controls and implications for global emission inventories, Environ. Sci. Technol., doi:10.1021/es203355v, 2012.

Felix, J. D. and Elliott, E. M.: The agricultural history of human-nitrogen interactions as recorded in ice core δ15N-NO3-, Geophys. Res. Lett., doi:10.1002/grl.50209, 2013.

Felix, J. D. and Elliott, E. M.: Isotopic composition of passively collected nitrogen dioxide emissions: Vehicle, soil and livestock source signatures, Atmos. Environ., doi:10.1016/j.atmosenv.2014.04.005, 2014.

Felix, J. D., Elliott, E. M., Avery, G. B., Kieber, R. J., Mead, R. N., Willey, J. D. and Mullaugh, K. M.: Isotopic composition of nitrate in sequential Hurricane Irene precipitation samples: Implications for changing NOx sources, Atmos. Environ., doi:10.1016/j.atmosenv.2015.01.075, 2015.

Fang, H., Walters, W. W., Mase, D., and Michalski, G.: iNRACM: incorporating ^{15}N into the Regional Atmospheric Chemistry Mechanism (RACM) for assessing the role photochemistry plays in controlling the isotopic composition of NO_x, NO_y, and atmospheric nitrate, Geosci. Model Dev., 14, 5001–5022, https://doi.org/10.5194/gmd-14-5001-2021, 2021.

Fibiger, D. L., Hastings, M. G., Lew, A. F. and Peltier, R. E.: Collection of NO and NO2 for isotopic analysis of NOx emissions, Anal. Chem., doi:10.1021/ac502968e, 2014.

Fraser, A., Goutail, F., McLinden, C. A., Melo, S. M. L. and Strong, K.: Lightning-produced NO2 observed by two ground-based UV-visible spectrometers at Vanscoy, Saskatchewan in August 2004, Atmos. Chem. Phys., doi:10.5194/acp-7-1683-2007, 2007.

Fujita, E. M., Croes, B. E., Bennett, C. L., Lawson, D. R., Lurmann, F. W. and Main, H. H.: Comparison of emission inventory and ambient concentration ratios of CO, NMOG, and NOx in California's South Coast Air Basin, J. Air Waste Manag. Assoc., doi:10.1080/10473289.1992.10466989, 1992.

Fujita, E. M., Campbell, D. E., Zielinska, B. B., Sagebiel, J. C., Bowen, J. L., Goliff, W. S., Stockwell, W. R. and Lawson, D. R.: Diurnal and weekday variations in the source contributions of ozone precursors in California's South Coast Air Basin, J. Air Waste Manag. Assoc., doi:10.1080/10473289.2003.10466226, 2003.

Deleted: Fang, H. & Michalski, G.: Incorporating 15N into the outputs of SMOKE version 4.6 as the emission input dataset for CMAQ version 5.2.1 for assessing the role emission sources plays in controlling the isotopic composition of NOx, NOy, and atmospheric nitrate. Geoscientific Model Development, 2020 (submitted).¶

Formatted: Justified

Formatted: Justified

Moved (insertion) [17]

Fujita, E. M., Stockwell, W. R., Campbell, D. E., Keislar, R. E. and Lawson, D. R.: Evolution of the magnitude and spatial extent of the weekend ozone effect in California's South Coast Air Basin, 1981–2000, J. Air Waste Manag. Assoc., doi:10.1080/10473289.2003.10466225, 2003.

Galbally, I. E. and Roy, C. R.: Loss of fixed nitrogen from soils by nitric oxide exhalation [11], Nature, doi:10.1038/275734a0, 1978.Gallardo, L. and Rodhe, H.: Oxidized nitrogen in the remote Pacific: The role of electrical discharges over the oceans, J. Atmos. Chem., doi:10.1023/A:1005738402496, 1997.

Gallardo, L. and Rodhe, H.: Oxidized nitrogen in the remote Pacific: The role of electrical discharges over the oceans, J. Atmos. Chem., doi:10.1023/A:1005738402496, 1997.

Galloway, J. N. and Cowling, E. B.: Reactive nitrogen and the world: 200 Years of change, in Ambio., 2002.

Galloway, J. N., Dentener, F. J., Capone, D. G., Boyer, E. W., Howarth, R. W., Seitzinger, S. P., Asner, G. P., Cleveland, C. C., Green, P. A., Holland, E. A., Karl, D. M., Michaels, A. F., Porter, J. H., Townsend, A. R. and Vörösmarty, C. J.: Nitrogen cycles: Past, present, and future, Biogeochemistry, doi:10.1007/s10533-004-0370-0, 2004.

Ganzeveld, L. N., Lelieveld, J., Dentener, F. J., Krol, M. C., Bouwman, A. J. and Roelofs, G. J.: Global soil-biogenic NOX emissions and the role of canopy processes, J. Geophys. Res. Atmos., doi:10.1029/2001JD001289, 2002.

Garten, C. T.: Nitrogen isotope composition of ammonium and nitrate in bulk precipitation and forest throughfall, Int. J. Environ. Anal. Chem., doi:10.1080/03067319208027017, 1992.

Gauss, M., Myhre, G., Isaksen, I. S. A., Grewe, V., Pitari, G., Wild, O., Collins, W. J., Dentener, F. J., Ellingsen, K., Gohar, L. K., Hauglustaine, D. A., Iachetti, D., Lamarque, J. F., Mancini, E., Mickley, L. J., Prather, M. J., Pyle, J. A., Sanderson, M. G., Shine, K. P., Stevenson, D. S., Sudo, K., Szopa, S. and Zeng, G.: Radiative forcing since preindustrial times due to ozone change in the troposphere and the lower stratosphere, Atmos. Chem. Phys., doi:10.5194/acp-6-575-2006, 2006.

Grell, G. A., Dudhia, J., & Stauffer, D. R.: A description of the fifth-generation Penn State/NCAR mesoscale model (MM5), NCAR Technical Note NCAR/TN-398+ STR, 1994.

Hall, S. J., Ogata, E. M., Weintraub, S. R., Baker, M. A., Ehleringer, J. R., Czimczik, C. I. and Bowling, D. R.: Convergence in nitrogen deposition and cryptic isotopic variation across urban and agricultural valleys in northern Utah, J. Geophys. Res. Biogeosciences, doi:10.1002/2016JG003354, 2016.

Hanson, P. J. and Lindberg, S. E.: Dry deposition of reactive nitrogen compounds: A review of leaf, canopy and non-foliar measurements, Atmos. Environ. Part A, Gen. Top., doi:10.1016/0960-1686(91)90020-8, 1991.

Formatted: Justified

Formatted: Justified

Formatted: Justified

Harley, R. A., McKeen, S. A., Pearson, J., Rodgers, M. O. and Lonneman, W. A.: Analysis of motor vehicle emissions during the Nashville/Middle Tennessee Ozone Study, J. Geophys. Res. Atmos., doi:10.1029/2000JD900677, 2001.

Heaton, T. H. E.: 15N14N ratios of nitrate and ammonium in rain at Pretoria, South Africa, Atmos. Environ., doi:10.1016/0004-6981(87)90080-1, 1987.

Heaton, T. H. E.: 15N/14N ratios of NOx from vehicle engines and coal-fired power stations, Tellus B, doi:10.1034/j.1600-0889.1990.00007.x-i1, 1990.

Hoering, T.: The isotopic composition of the ammonia and the nitrate ion in rain, Geochim. Cosmochim. Acta, doi:10.1016/0016-7037(57)90021-2, 1957.

Houlton, B. Z., Boyer, E., Finzi, A., Galloway, J., Leach, A., Liptzin, D., Melillo, J., Rosenstock, T. S., Sobota, D. and Townsend, A. R.: Intentional versus unintentional nitrogen use in the United States: Trends, efficiency and implications, Biogeochemistry, doi:10.1007/s10533-012-9801-5, 2013.

Houyoux, M.: Clean Air Interstate Rule Emissions Inventory Technical Support Document. US EPA, 2005.

Hudman, R. C., Moore, N. E., Mebust, A. K., Martin, R. V., Russell, A. R., Valin, L. C. and Cohen, R. C.: Steps towards a mechanistic model of global soil nitric oxide emissions: Implementation and space based-constraints, Atmos. Chem. Phys., doi:10.5194/acp-12-7779-2012, 2012.

Huntrieser, H., Schlager, H., Feigl, C. and Höller, H.: Transport and production of NOX in electrified thunderstorms: Survey of previous studies and new observations at midlatitudes, J. Geophys. Res. Atmos., doi:10.1029/98JD02353, 1998.

Huntrieser, H., Feigl, C., Schlager, H., Schröder, F., Gerbig, C., van Velthoven, P., Flatøy, F., Théry, C., Petzold, A., Höller, H. and Schumann, U.: Airborne measurements of NOx, tracer species, and small particles during the European lightning nitrogen oxides experiment, J. Geophys. Res. Atmos., doi:10.1029/2000jd000209, 2002.

Ingalls, M. N.: On-road vehicle emission factors from measurements in a Los Angeles area tunnel, in Proceedings - A&WMA Annual Meeting., 1989.

Jacob, D. J. and Wofsy, S. C.: Budgets of reactive nitrogen, hydrocarbons, and ozone over the Amazon forest during the wet season, J. Geophys. Res., doi:10.1029/jd095id10p16737, 1990.

Jaeglé, L., Steinberger, L., Martin, R. V. and Chance, K.: Global partitioning of NOx sources using satellite observations: Relative roles of fossil fuel combustion, biomass burning and soil emissions, in Faraday Discussions., 2005.

Johansson, C.: Pine forest: a negligible sink for atmospheric NO x in rural Sweden , Tellus B Chem. Phys. Meteorol., doi:10.3402/tellusb.v39i5.15360, 1987.

Kim, S. W., Heckel, A., Frost, G. J., Richter, A., Gleason, J., Burrows, J. P., McKeen, S., Hsie, E. Y., Granier, C. and Trainer, M.: NO2 columns in the western United States observed from space and simulated by a regional chemistry model and their implications for NO x emissions, J. Geophys. Res. Atmos., doi:10.1029/2008JD011343, 2009.

Koike, M., Kondo, Y., Kita, K., Takegawa, N., Nishi, N., Kashihara, T., Kawakami, S., Kudoh, S., Blake, D., Shirai, T., Liley, B., Ko, M. K., Miyazaki, Y., Kawasaki, Z. and Ogawa, T.: Measurements of reactive nitrogen produced by tropical thunderstorms during BIBLE-C, J. Geophys. Res. Atmos., doi:10.1029/2006JD008193, 2007.

Laughner, J. L., & Cohen, R. C. (2019). Direct observation of changing NOx lifetime in North American cities. *Science*, *366*(6466), 723-727.

Lawrence, M. G., Chameides, W. L., Kasibhatla, P. S., Levy, H. and Moxim, W.: Lightning and atmospheric chemistry: The rate of atmospheric NO production, in Handbook of Atmospheric Electrodynamics., 2017.

Lerdau, M. T., Munger, J. W. and Jacob, D. J.: The NO2 flux conundrum, Science (80-.)., doi:10.1126/science.289.5488.2291, 2000.

Levy, H., Moxim, W. J. and Kasibhatla, P. S.: A global three-dimensional time-dependent lightning source of tropospheric NOx, J. Geophys. Res. Atmos., doi:10.1029/96jd02341, 1996.

Li, D. and Wang, X.: Nitrogen isotopic signature of soil-released nitric oxide (NO) after fertilizer application, Atmos. Environ., doi:10.1016/j.atmosenv.2008.01.042, 2008.

Li, Y., Schichtel, B. A., Walker, J. T., Schwede, D. B., Chen, X., Lehmann, C. M. B., Puchalski, M. A., Gay, D. A. and Collett, J. L.: Increasing importance of deposition of reduced nitrogen in the United States, Proc. Natl. Acad. Sci. U. S. A., doi:10.1073/pnas.1525736113, 2016.

Liao, T., Gui, K., Jiang, W., Wang, S., Wang, B., Zeng, Z., Che, H., Wang, Y. and Sun, Y.: Air stagnation and its impact on air quality during winter in Sichuan and Chongqing, southwestern China, Sci. Total Environ., doi:10.1016/j.scitotenv.2018.04.122, 2018.

Lighty, J. A. S., Veranth, J. M. and Sarofim, A. F.: Combustion aerosols: Factors governing their size and composition and implications to human health, J. Air Waste Manag. Assoc., doi:10.1080/10473289.2000.10464197, 2000.

Liu, L., Guo, J., Miao, Y., Liu, L., Li, J., Chen, D., He, J. and Cui, C.: Elucidating the relationship between aerosol concentration and summertime boundary layer structure in central China, Environ. Pollut., doi:10.1016/j.envpol.2018.06.008, 2018.

Formatted: Justified

Formatted: Justified

Lu, Z., Streets, D. G., De Foy, B., Lamsal, L. N., Duncan, B. N. and Xing, J.: Emissions of nitrogen oxides from US urban areas: Estimation from Ozone Monitoring Instrument retrievals for 2005-2014, Atmos. Chem. Phys., doi:10.5194/acp-15-10367-2015, 2015.

Ludwig, J., Meixner, F. X., Vogel, B. and Forstner, J.: Soil-air exchange of nitric oxide: An overview of processes, environmental factors, and modeling studies, Biogeochemistry, doi:10.1023/A:1006424330555, 2001.

Martin, R. V., Sauvage, B., Folkins, I., Sioris, C. E., Booone, C., Bernath, P. and Ziemke, J.: Space-based constraints on the production of nitric oxide by lightning, J. Geophys. Res. Atmos., doi:10.1029/2006JD007831, 2007.

Mase, D. F.: A coupled modeling and observational approach to understanding oxygen-18 in atmospheric nitrate, Ph. D. thesis, Purdue University, United States of America, 2010.

McDonald, B. C., McKeen, S. A., Cui, Y. Y., Ahmadov, R., Kim, S. W., Frost, G. J., ... & Trainer, M.: Modeling ozone in the eastern US using a fuel-based mobile source emissions inventory, Environmental science & technology, 52(13), 7360-7370, 2018.

Miao, Y., Guo, J., Liu, S., Zhao, C., Li, X., Zhang, G., Wei, W. and Ma, Y.: Impacts of synoptic condition and planetary boundary layer structure on the trans-boundary aerosol transport from Beijing-Tianjin-Hebei region to northeast China, Atmos. Environ., doi:10.1016/j.atmosenv.2018.03.005, 2018.

Miao, Y., Li, J., Miao, S., Che, H., Wang, Y., Zhang, X., Zhu, R. and Liu, S.: Interaction Between Planetary Boundary Layer and PM2.5 Pollution in Megacities in China: a Review, Curr. Pollut. Reports, doi:10.1007/s40726-019-00124-5, 2019.

Miller, D. J., Wojtal, P. K., Clark, S. C. and Hastings, M. G.: Vehicle NOx emission plume isotopic signatures: Spatial variability across the eastern United States, J. Geophys. Res., doi:10.1002/2016JD025877, 2017.

Miller, D. J., Chai, J., Guo, F., Dell, C. J., Karsten, H. and Hastings, M. G.: Isotopic Composition of In Situ Soil NOx Emissions in Manure-Fertilized Cropland, Geophys. Res. Lett., doi:10.1029/2018GL079619, 2018.

Moore, H.: The isotopic composition of ammonia, nitrogen dioxide and nitrate in the atmosphere, Atmos. Environ., doi:10.1016/0004-6981(77)90102-0, 1977.

Muller, J. F.: Geographical distribution and seasonal variation of surface emissions and deposition velocities of atmospheric trace gases, J. Geophys. Res., doi:10.1029/91JD02757, 1992.

Müller, J.-F. and Stavrakou, T.: Inversion of CO and NOx emissions using the adjoint of the IMAGES model, Atmos. Chem. Phys., doi:10.5194/acp-5-1157-2005, 2005.

Formatted: Justified

Formatted: Left

Moved up [16]: G.,

Moved up [17]: ., Walters, W. W.,

Deleted: Michalski,

Deleted: Fang, H

Deleted: & Mase, D.: i_N RACM: Incorporating ^{15}N into the Regional Atmospheric Chemistry Mechanism (RACM) for assessing the role photochemistry plays in controlling the isotopic composition of NO_x, NO_y, and atmospheric nitrate, Geoscientific Model Development Discussions, 1-47, 2020.¶ ¶

Formatted: Justified

Murray, L. T.: Lightning NOx and Impacts on Air Quality, Curr. Pollut. Reports, doi:10.1007/s40726-016-0031-7, 2016.

National Centers for Environmental Information: U.S. Wind Climatology, Available from: https://www.ncdc.noaa.gov/societal-impacts/wind/, 2019.

National Centers for Environmental Information: Model Datasets, available from: https://www.ncdc.noaa.gov/data-access/model-data/model-datasets, 2019.

Occhipinti, C., Aneja, V. P., Showers, W. and Niyogi, D.: Back-trajectory analysis and source-receptor relationships: Particulate matter and nitrogen isotopic composition in rainwater, Journal of the Air and Waste Management Association., 2008.

Oke, T. R.: Boundary Layer Climates., 2002.

Ott, L. E., Pickering, K. E., Stenchikov, G. L., Huntrieser, H. and Schumann, U.: Effects of lightning NOx production during the 21 July European Lightning Nitrogen Oxides Project storm studied with a three-dimensional cloud-scale chemical transport model, J. Geophys. Res. Atmos., doi:10.1029/2006JD007365, 2007.

Parrish, D. D.: Critical evaluation of US on-road vehicle emission inventories, Atmos. Environ., doi:10.1016/j.atmosenv.2005.11.033, 2006.

Pearson, J., Wells, D. M., Seller, K. J., Bennett, A., Soares, A., Woodall, J. and Ingrouille, M. J.: Traffic exposure increases natural 15N and heavy metal concentrations in mosses, New Phytol., doi:10.1046/j.1469-8137.2000.00702.x, 2000.

Pierce, T. E.: Reconsideration of the Emission Factors assumed in BEIS3 for Three USGS Vegetation Categories: Shrubland, Coniferous Forest, and Deciduous Forest, 2001.

Pierson, W. R., Gertler, A. W. and Bradow, R. L.: Comparison of the scaqs tunnel study with other onroad vehicle emission data, J. Air Waste Manag. Assoc., doi:10.1080/10473289.1990.10466799, 1990.

Pierson, W. R., Gertler, A. W., Robinson, N. F., Sagebiel, J. C., Zielinska, B., Bishop, G. A., Stedman, D. H., Zweidinger, R. B. and Ray, W. D.: Real-world automotive emissions - summary of studies in the Fort McHenry and Tuscarora Mountain Tunnels, in Atmospheric Environment., 1996.

Pilegaard, K.: Processes regulating nitric oxide emissions from soils, Philos. Trans. R. Soc. B Biol. Sci., doi:10.1098/rstb.2013.0126, 2013.

Potter, C. S., Matson, P. A., Vitousek, P. M. and Davidson, E. A.: Process modeling of controls on nitrogen trace gas emissions from soils worldwide, J. Geophys. Res. Atmos., doi:10.1029/95JD02028, 1996.

Formatted: Left

Deleted: in

Formatted: Justified

Pouliot, G., & Pierce, T. E.: Integration of the Model of Emissions of Gases and Aerosols from Nature (MEGAN) into the CMAQ Modeling System, in: 18th International Emission Inventory Conference, Baltimore, Maryland, 14 April 2009, 14-17, 2009.

Redling, K., Elliott, E., Bain, D. and Sherwell, J.: Highway contributions to reactive nitrogen deposition: Tracing the fate of vehicular NOx using stable isotopes and plant biomonitors, Biogeochemistry, doi:10.1007/s10533-013-9857-x, 2013.

Ridley, B. A., Dye, J. E., Walega, J. G., Zheng, J., Grahek, F. E. and Rison, W.: On the production of active nitrogen by thunderstorms over New Mexico, J. Geophys. Res. Atmos., doi:10.1029/96jd01706, 1996.

Ridley, B., Ott, L., Pickering, K., Emmons, L., Montzka, D., Weinheimer, A., Knapp, D., Grahek, F., Li, L., Heymsfield, G., McGill, M., Kucera, P., Mahoney, M. J., Baumgardner, D., Schultz, M. and Brasseur, G.: Florida thunderstorms: A faucet of reactive nitrogen to the upper troposphere, J. Geophys. Res. D Atmos., doi:10.1029/2004JD004769, 2004.

Riha, K. M.: The use of stable isotopes to constrain the nitrogen cycle, Ph. D. thesis, Purdue University, United States of America, 2013.

Russell, K. M., Galloway, J. N., MacKo, S. A., Moody, J. L. and Scudlark, J. R.: Sources of nitrogen in wet deposition to the Chesapeake Bay region, Atmos. Environ., doi:10.1016/S1352-2310(98)00044-2, 1998.

Savard, M. M., Bégin, C., Smirnoff, A., Marion, J. and Rioux-Paquette, E.: Tree-ring nitrogen isotopes reflect anthropogenic NOx emissions and climatic effects, Environ. Sci. Technol., doi:10.1021/es802437k, 2009.

Savard, M. M., Cole, A., Smirnoff, A. and Vet, R.: Δ15N values of atmospheric N species simultaneously collected using sector-based samplers distant from sources – Isotopic inheritance and fractionation, Atmos. Environ., doi:10.1016/j.atmosenv.2017.05.010, 2017.

Sawyer, R. F., Harley, R. A., Cadle, S. H., Norbeck, J. M., Slott, R. and Bravo, H. A.: Mobile sources critical review: 1998 NARSTO assessment, Atmos. Environ., doi:10.1016/S1352-2310(99)00463-X, 2000.

Scholes, M. C., Martin, R., Scholes, R. J., Parsons, D. and Winstead, E.: NO and N2O emissions from savanna soils following the first simulated rains of the season, Nutr. Cycl. Agroecosystems, doi:10.1023/a:1009781420199, 1997.

Schumann, U., Kurz, C., Schlager, H., Huntrieser, H., Emmons, L., Labrador, L., Meijer, E., Ulanovsky, A. and Viciani, S.: Towards a robust estimate of the global lightning nitrogen oxides source rate and its error bound, in European Space Agency, (Special Publication) ESA SP., 2006.

Schumann, U. and Huntrieser, H.: The global lightning-induced nitrogen oxides source, Atmos. Chem. Phys., doi:10.5194/acp-7-3823-2007, 2007.

Moved down [18]: Riha, K. M.: The use of stable isotopes to constrain the nitrogen cycle, Ph. D. thesis, Purdue University, United States of America, 2013.¶
¶

Moved (insertion) [18]

Formatted: Left

Formatted: Justified

Schwartz, S. E.: The Whitehouse effect - Shortwave radiative forcing of climate by anthropogenic aerosols: An overview, J. Aerosol Sci., doi:10.1016/0021-8502(95)00533-1, 1996.

Schwede, D., Pouliot, G. and Pierce, T.: Changes to the biogenic emissions inventory system version 3 (BEIS3), in 4th Annual CMAS User's Conference., 2005.

Selden, T. M., Forrest, A. S., & Lockhart, J. E.: Analyzing the reductions in US air pollution emissions: 1970 to 1990, Land Economics, 1-21, doi: 10.2307/3146990, 1999.

Shepherd, M. F., Barzetti, S. and Hastie, D. R.: The production of atmospheric NOx and N2O from a fertilized agricultural soil, Atmos. Environ. Part A, Gen. Top., doi:10.1016/0960-1686(91)90277-E, 1991.

Shu, L., Xie, M., Gao, D., Wang, T., Fang, D., Liu, Q., Huang, A. and Peng, L.: Regional severe particle pollution and its association with synoptic weather patterns in the Yangtze River Delta region, China, Atmos. Chem. Phys., doi:10.5194/acp-17-12871-2017, 2017.

Singer, B. C. and Harley, R. A.: A Fuel-Based Motor Vehicle Emission Inventory, J. Air Waste Manag. Assoc., doi:10.1080/10473289.1996.10467492, 1996.

Singer, B. C. and Harley, R. A.: A fuel-based inventory of motor vehicle exhaust emissions in the Los Angeles area during summer 1997, Atmos. Environ., doi:10.1016/S1352-2310(99)00358-1, 2000.

Skamarock, W. C., Dye, J. E., Defer, E., Barth, M. C., Stith, J. L., Ridley, B. A. and Baumann, K.: Observational- and modeling-based budget of lightning-produced NOx in a continental thunderstorm, J. Geophys. Res. Atmos., doi:10.1029/2002jd002163, 2003.

Slovik, S., Siegmund, A., Fuhrer, H. W. and Heber, U.: Stomatal uptake of SO2, NOx and O3 by spruce crowns (Picea abies) and canopy damage in Central Europe, New Phytol., doi:10.1111/j.1469-8137.1996.tb01884.x, 1996.

Snape, C. E., Sun, C., Fallick, A. E., Irons, R. and Haskell, J.: Potential of stable nitrogen isotope ratio measurements to resolve fuel and thermal NOx in coal combustion, Fuel Chem. Div. Prepr., 2003.

Snyder, J. P.: Map projections - a working manual, US Geol. Surv. Prof. Pap., 1987.

Spak, S., Holloway, T., Mednick, A., & Stone, B.: Evaluation of Bottom-Up Mobile Emissions Inventories in the Upper Midwest, in: American Geophysical Union Fall Meeting, San Francisco, California, 10-14 Dec 2007, 2007.

Srivastava, R. K., Neuffer, W., Grano, D., Khan, S., Staudt, J. E. and Jozewicz, W.: Controlling NO x emission from industrial sources, Environ. Prog., doi:10.1002/ep.10063, 2005.

Staudt, A. C., Jacob, D. J., Ravetta, F., Logan, J. A., Bachiochi, D., Sandholm, S., Ridley, B., Singh, H. B. and Talbot, B.: Sources and chemistry of nitrogen oxides over the tropical Pacific, J. Geophys. Res. Atmos., doi:10.1029/2002jd002139, 2003.

Stavrakou, T., Müller, J. F., Boersma, K. F., Van Der A., R. J., Kurokawa, J., Ohara, T. and Zhang, Q.: Key chemical NOx sink uncertainties and how they influence top-down emissions of nitrogen oxides, Atmos. Chem. Phys., doi:10.5194/acp-13-9057-2013, 2013.

Stehfest, E. and Bouwman, L.: N2O and NO emission from agricultural fields and soils under natural vegetation: Summarizing available measurement data and modeling of global annual emissions, Nutr. Cycl. Agroecosystems, doi:10.1007/s10705-006-9000-7, 2006.

Stevenson, D. S., Dentener, F. J., Schultz, M. G., Ellingsen, K., van Noije, T. P. C., Wild, O., Zeng, G., Amann, M., Atherton, C. S., Bell, N., Bergmann, D. J., Bey, I., Butler, T., Cofala, J., Collins, W. J., Derwent, R. G., Doherty, R. M., Drevet, J., Eskes, H. J., Fiore, A. M., Gauss, M., Hauglustaine, D. A., Horowitz, L. W., Isaksen, I. S. A., Krol, M. C., Lamarque, J. F., Lawrence, M. G., Montanaro, V., Müller, J. F., Pitari, G., Prather, M. J., Pyle, J. A., Rast, S., Rodriquez, J. M., Sanderson, M. G., Savage, N. H., Shindell, D. T., Strahan, S. E., Sudo, K. and Szopa, S.: Multimodel ensemble simulations of present-day and near-future tropospheric ozone, J. Geophys. Res. Atmos., doi:10.1029/2005JD006338, 2006.

The Institute for the Environment - The University of North Carolina at Chapel Hill: SMOKE v4.5 User's Manual, Available from: https://www.cmascenter.org/smoke/documentation/4.5/html/, 2017.

Thoene, B., Rennenberg, H. and Weber, P.: Absorption of atmospheric NO2 by spruce (Picea abies) trees: II. Parameterization of NO2 fluxes by controlled dynamic chamber experiments, New Phytol., doi:10.1111/j.1469-8137.1996.tb04630.x, 1996.

Thomas, R. J., Krehbiel, P. R., Rison, W., Hamlin, T., Boccippio, D. J., Goodman, S. J. and Christian, H. J.: Comparison of ground-based 3-dimensional lightning mapping observations with satellite-based LIS observations in Oklahoma, Geophys. Res. Lett., doi:10.1029/1999GL010845, 2000.

Tie, X., Zhang, R., Brasseur, G. and Lei, W.: Global NOx production by lightning, J. Atmos. Chem., doi:10.1023/A:1016145719608, 2002.

Tost, H., Jöckel, P. and Lelieveld, J.: Lightning and convection parameterisations - Uncertainties in global modelling, Atmos. Chem. Phys., doi:10.5194/acp-7-4553-2007, 2007.

United States Census Bureau: 2007−2011 American Community Survey 5-Year Estimates, travel time to work by zip code, table B08303, Available from: https://www.census.gov/programs-surveys/acs/technical-documentation/table-and-geography-changes/2011/5-year.html, 2019.

United States Energy Information Administration: Electricity, Available from: https://www.eia.gov/electricity/data/eia860/, 2017a.

United States Energy Information Administration: U.S. electric generating capacity increase in 2016 was largest net change since 2011, Available from: https://www.eia.gov/todayinenergy/detail.php?id=30112, 2017b.

United States Environmental Protection Agency: National Emissions Inventory (NEI), Available from: https://www.epa.gov/air-emissions-inventories/national-emissions-inventory-nei, 2014.

United States Environmental Protection Agency: Biogenic Emissions Landuse Database, Available from: https://www.epa.gov/air-emissions-modeling/biogenic-emissions-landuse-database-version-3-beld3, 2018a.

United States Environmental Protection Agency: 2002 National Emissions Inventory (NEI) Booklet, Available from: https://archive.epa.gov/epa/air-emissions-inventories/2002-national-emissions-inventory-nei-booklet.html, 2018b

US Environmental Protection Agency: User's Guide to MOBILE6.1 and MOBILE6.2 Mobile Source Emission Factor Model, Tech. Rep. EPA420-R-03-010, 2003.

Van Noije, T. P. C., Eskes, H. J., Dentener, F. J., Stevenson, D. S., Ellingsen, K., Schultz, M. G., Wild, O., Amann, M., Atherton, C. S., Bergmann, D. J., Bey, I., Boersma, K. F., Butler, T., Cofala, J., Drevet, J., Fiore, A. M., Gauss, M., Hauglustaine, D. A., Horowitz, L. W., Isaksen, I. S. A., Krol, M. C., Lamarque, J. F., Lawrence, M. G., Martin, R. V., Montanaro, V., Müller, J. F., Pitari, G., Prather, M. J., Pyle, J. A., Richter, A., Rodriguez, J. M., Savage, N. H., Strahan, S. E., Sudo, K., Szopa, S. and Van Roozendael, M.: Multi-model ensemble simulations of tropospheric NO2 compared with GOME retrievals for the year 2000, Atmos. Chem. Phys., doi:10.5194/acp-6-2943-2006, 2006.

Vukovich, J., & Pierce, T.: The implementation of BEIS3 within the SMOKE modeling framework, in: Proceedings of the 11th International Emissions Inventory Conference, Atlanta, Georgia, 15 April 2002, 15-18, 2002.

Walters, W. W., Goodwin, S. R. and Michalski, G.: Nitrogen stable isotope composition ($\delta^{15}N$) of vehicle-emitted NOx, Environ. Sci. Technol., doi:10.1021/es505580v, 2015a.

Walters, W. W., Tharp, B. D., Fang, H., Kozak, B. J. and Michalski, G.: Nitrogen Isotope Composition of Thermally Produced NOx from Various Fossil-Fuel Combustion Sources, Environ. Sci. Technol., doi:10.1021/acs.est.5b02769, 2015b.

Walters, W. W. and Michalski, G.: Theoretical calculation of nitrogen isotope equilibrium exchange fractionation factors for various NOy molecules, Geochim. Cosmochim. Acta, doi:10.1016/j.gca.2015.05.029, 2015.

Walters, W. W., Simonini, D. S. and Michalski, G.: Nitrogen isotope exchange between NO and NO2 and its implications for δ15N variations in tropospheric NOx and atmospheric nitrate, Geophys. Res. Lett., doi:10.1002/2015GL066438, 2016.

Deleted: 2018

Formatted: Superscript

Walters, W. W., Fang, H. and Michalski, G.: Summertime diurnal variations in the isotopic composition of atmospheric nitrogen dioxide at a small midwestern United States city, Atmos. Environ., doi:10.1016/j.atmosenv.2018.01.047, 2018.

Weber, P. and Rennenberg, H.: Dependency of nitrogen dioxide (NO2) fluxes to wheat (Triticum aestivum L.) leaves from NO2 concentration, light intensity, temperature and relative humidity determined from controlled dynamic chamber experiments, Atmos. Environ., doi:10.1016/1352-2310(96)00008-8, 1996.

Wong, S., Wang, W. C., Isaksen, I. S. A., Berntsen, T. K. and Sundet, J. K.: A global climate-chemistry model study of present-day tropospheric chemistry and radiative forcing from changes in tropospheric O3 since the preindustrial period, J. Geophys. Res. D Atmos., doi:10.1029/2003JD003998, 2004.

Xing, J., Pleim, J., Mathur, R., Pouliot, G., Hogrefe, C., Gan, C. M. and Wei, C.: Historical gaseous and primary aerosol emissions in the United States from 1990 to 2010, Atmos. Chem. Phys., doi:10.5194/acp-13-7531-2013, 2013.

Yan, X., Ohara, T. and Akimoto, H.: Statistical modeling of global soil NOX emissions, Global Biogeochem. Cycles, doi:10.1029/2004GB002276, 2005.

Yienger, J. J. and Levy, H.: Empirical model of global soil-biogenic NOx emissions, J. Geophys. Res., doi:10.1029/95jd00370, 1995.

Yu, Z. and Elliott, E. M.: Novel Method for Nitrogen Isotopic Analysis of Soil-Emitted Nitric Oxide, Environ. Sci. Technol., doi:10.1021/acs.est.7b00592, 2017.

Zörner, J., Penning de Vries, M. J. M., Beirle, S., Sihler, H., Veres, P. R., Williams, J. and Wagner, T.: Multi-satellite sensor study on precipitation-induced emission pulses of NO_x from soils in semi-arid ecosystems, Atmos. Chem. Phys. Discuss., doi:10.5194/acp-2016-93, 2016.

Formatted: Left

Formatted: Font: Not Italic

Deleted: ¶

Page 3: [1] Deleted Huan Fang 1/5/22 5:36:00 PM

Page 3: [2] Deleted Huan Fang 1/5/22 5:36:00 PM

Page 5: [3] Deleted Huan Fang 1/5/22 5:36:00 PM

Page 5: [4] Formatted Huan Fang 1/5/22 5:36:00 PM

Outline numbered + Level: 1 + Numbering Style: 1, 2, 3, … + Start at: 1 + Alignment: Left + Aligned at: 0" + Indent at: 0.25"

Page 5: [5] Deleted Huan Fang 1/5/22 5:36:00 PM

Page 5: [6] Deleted Huan Fang 1/5/22 5:36:00 PM

Page 5: [7] Deleted Huan Fang 1/5/22 5:36:00 PM

Page 5: [8] Deleted Huan Fang 1/5/22 5:36:00 PM

Page 10: [9] Deleted Huan Fang 1/5/22 5:36:00 PM

Page 10: [10] Deleted Huan Fang 1/5/22 5:36:00 PM

Page 10: [11] Deleted Huan Fang 1/5/22 5:36:00 PM

Page 11: [12] Deleted Huan Fang 1/5/22 5:36:00 PM

Page 11: [12] Deleted Huan Fang 1/5/22 5:36:00 PM

Page 11: [12] Deleted Huan Fang 1/5/22 5:36:00 PM

Page 11: [12] Deleted Huan Fang 1/5/22 5:36:00 PM

Page 11: [12] Deleted Huan Fang 1/5/22 5:36:00 PM

Page 11: [12] Deleted Huan Fang 1/5/22 5:36:00 PM

Page 11: [12] Deleted Huan Fang 1/5/22 5:36:00 PM

Page 11: [12] Deleted Huan Fang 1/5/22 5:36:00 PM

Page 11: [12] Deleted Huan Fang 1/5/22 5:36:00 PM

Page 11: [13] Formatted Huan Fang 1/5/22 5:36:00 PM

Font: 12 pt

Page 11: [13] Formatted Huan Fang 1/5/22 5:36:00 PM

Font: 12 pt

Page 11: [14] Formatted Huan Fang 1/5/22 5:36:00 PM

Font: Times New Roman, 12 pt

Page 11: [14] Formatted Huan Fang 1/5/22 5:36:00 PM

Font: Times New Roman, 12 pt

Page 11: [15] Deleted Huan Fang 1/5/22 5:36:00 PM

Page 11: [16] Deleted Huan Fang 1/5/22 5:36:00 PM

Page 11: [16] Deleted Huan Fang 1/5/22 5:36:00 PM

Page 11: [16] Deleted Huan Fang 1/5/22 5:36:00 PM

Page 11: [16] Deleted Huan Fang 1/5/22 5:36:00 PM

Page 11: [16] Deleted Huan Fang 1/5/22 5:36:00 PM

Page 16: [17] Deleted Huan Fang 1/5/22 5:36:00 PM

Page 16: [17] Deleted Huan Fang 1/5/22 5:36:00 PM

Page 16: [17] Deleted Huan Fang 1/5/22 5:36:00 PM

Page 16: [17] Deleted Huan Fang 1/5/22 5:36:00 PM

Page 16: [17] Deleted Huan Fang 1/5/22 5:36:00 PM

Page 16: [17] Deleted Huan Fang 1/5/22 5:36:00 PM

Page 16: [17] Deleted Huan Fang 1/5/22 5:36:00 PM

Page 16: [17] Deleted Huan Fang 1/5/22 5:36:00 PM

Page 16: [18] Deleted Huan Fang 1/5/22 5:36:00 PM

Page 16: [18] Deleted Huan Fang 1/5/22 5:36:00 PM

Page 16: [18] Deleted Huan Fang 1/5/22 5:36:00 PM

Page 16: [18] Deleted Huan Fang 1/5/22 5:36:00 PM

Page 16: [18] Deleted Huan Fang 1/5/22 5:36:00 PM

Page 16: [18] Deleted Huan Fang 1/5/22 5:36:00 PM

Page 16: [18] Deleted Huan Fang 1/5/22 5:36:00 PM

Page 16: [18] Deleted Huan Fang 1/5/22 5:36:00 PM

Page 16: [18] Deleted Huan Fang 1/5/22 5:36:00 PM

Page 16: [18] Deleted Huan Fang 1/5/22 5:36:00 PM

Page 16: [18] Deleted Huan Fang 1/5/22 5:36:00 PM

Page 16: [18] Deleted Huan Fang 1/5/22 5:36:00 PM

Page 16: [18] Deleted Huan Fang 1/5/22 5:36:00 PM

Page 16: [18] Deleted Huan Fang 1/5/22 5:36:00 PM

Page 16: [18] Deleted Huan Fang 1/5/22 5:36:00 PM

Page 16: [18] Deleted Huan Fang 1/5/22 5:36:00 PM

Page 16: [18] Deleted Huan Fang 1/5/22 5:36:00 PM

Page 16: [18] Deleted Huan Fang 1/5/22 5:36:00 PM

Page 16: [18] Deleted Huan Fang 1/5/22 5:36:00 PM

Page 16: [18] Deleted Huan Fang 1/5/22 5:36:00 PM

Page 16: [18] Deleted Huan Fang 1/5/22 5:36:00 PM

Page 16: [19] Deleted Huan Fang 1/5/22 5:36:00 PM

Page 16: [19] Deleted Huan Fang 1/5/22 5:36:00 PM

Page 16: [19] Deleted Huan Fang 1/5/22 5:36:00 PM

Page 16: [19] Deleted Huan Fang 1/5/22 5:36:00 PM

Page 16: [20] Deleted Huan Fang 1/5/22 5:36:00 PM

Page 16: [20] Deleted Huan Fang 1/5/22 5:36:00 PM

Page 16: [20] Deleted Huan Fang 1/5/22 5:36:00 PM

Page 16: [20] Deleted Huan Fang 1/5/22 5:36:00 PM

Page 16: [20] Deleted Huan Fang 1/5/22 5:36:00 PM

Page 16: [21] Deleted Huan Fang 1/5/22 5:36:00 PM

Page 16: [21] Deleted Huan Fang 1/5/22 5:36:00 PM

Page 16: [21] Deleted Huan Fang 1/5/22 5:36:00 PM

Page 16: [21] Deleted Huan Fang 1/5/22 5:36:00 PM

Page 22: [22] Deleted Huan Fang 1/5/22 5:36:00 PM

Page 23: [23] Deleted Huan Fang 1/5/22 5:36:00 PM

Page 23: [24] Deleted Huan Fang 1/5/22 5:36:00 PM

Page 23: [25] Formatted Huan Fang 1/5/22 5:36:00 PM

Font: Times New Roman, Font color: Auto